Prediction of clog time of amorphous silica in the pipes of the wells from Los Humeros geothermal field – A new geochemical model along with a computational algorithm

Predicción del tiempo de obturación con sílice amorfa en los tubos de los pozos del campo geotérmico de Los Humeros – Nuevo modelo geoquímico en conjunto con un algoritmo computacional

Sumit **Mishra**[1,*], Eduardo **González-Partida**[1], Antoni **Camprubí**[2], Sanjeet K. **Verma**[3], Kailasa **Pandarinath**[4], Renée **Pérez-Rodríguez**[5], Joseph **Madondo**[1]

[1] Centro de Geociencias, Universidad Nacional Autónoma de México, Boulevard Juriquilla 3001, 76230, Juriquilla, Querétaro, México

[2] Instituto de Geología, Universidad Nacional Autónoma de México, Ciudad Universitaria, Coyoacán, 04510, CDMX, México.

[3] División de Geociencias Aplicadas, Instituto Potosino de Investigación Científica y Tecnológica, A.C. Camino a la Presa San José # 2055, Col. Lomas 4a Sec., 78216, San Luis Potosí, SLP, México.

[4] Instituto de Energías Renovables, Universidad Nacional Autónoma de México, Privada Xochicalco s/n, Centro, 62580 Temixco, Morelos, México.

[5] Geochemical Research and Engineering, Inc., 75 Cormack Crescent, Edmonton, Alberta T2R2E6, Canada.

* Corresponding author: (S. Mishra)
smpsgeo@geociencias.unam.mx

How to cite this article:
Mishra, S., González-Partida, E., Camprubí, A., Verma, S.K., Pandarinath, K., Pérez-Rodríguez, R., Madondo, J., 2024, Prediction of clog time of amorphous silica in the pipes of the wells from Los Humeros geothermal field – A new geochemical model along with a computational algorithm: Boletín de la Sociedad Geológica Mexicana, 76 (1), A020124. http://dx.doi.org/10.18268/BSGM2024v76n1a020124

Manuscript received: October 15, 2023.
Corrected manuscript received: January 25, 2024.
Manuscript accepted: February 2, 2024.

Peer Reviewing under the responsibility of Universidad Nacional Autónoma de México.

ABSTRACT

The primary objective of this article is to introduce a physicochemical model along with a computational algorithm that is valuable for quantifying the occurrence of silica scaling and fouling within geothermal production wells. This model utilizes two-phase flow parameters, temperature and pressure profiles, as well as brine composition to forecast the timing of production pipe constriction caused by amorphous silica deposition over time. The model is applicable to systems with temperatures ranging from 270°C to 305°C, vapor pressures ranging from 55 to 93 bars, and enthalpies ranging from 1189 kJ/kg to 1400 kJ/kg. The predictive model was calibrated using data gathered from six distinct wells within the Los Humeros geothermal field in Mexico, and subsequently, it was applied to forecast outcomes in two additional wells. When the conditions of temperature, pressure, and enthalpy remain relatively constant throughout the production process, the model developed in this study accurately predicts the times at which a certain percentage of pipe sealing occurs in wells with high volumetric fractions of liquid (ε_l>0.5) and temperatures between 270°C and 305°C. The prediction error is less than 3%.

Keywords: timing of sealing, silica scaling, kinetic precipitation, geothermal field.

RESUMEN

El objetivo principal de este artículo es presentar un modelo fisicoquímico junto con un algoritmo computacional que resulta valioso para cuantificar la presencia de incrustaciones y obstrucciones de sílice en pozos de producción geotérmica. Este modelo utiliza parámetros de flujo bifásico, perfiles de temperatura y presión, así como la composición de la salmuera para prever el momento de constricción de la tubería de producción causada por la deposición de sílice amorfa con el tiempo. El modelo es aplicable a sistemas con temperaturas que van desde 270°C a 305°C, presiones de vapor que van de 55 a 93 bares y entalpías que van de 1189 kJ/kg a 1400 kJ/kg. El modelo predictivo se calibró utilizando datos recopilados de seis pozos distintos dentro del campo geotérmico de Los Humeros en México y, posteriormente, se aplicó para prever resultados en dos pozos adicionales. Cuando las condiciones de temperatura, presión y entalpía permanecen relativamente constantes durante el proceso de producción, el modelo desarrollado en este estudio predice con precisión los momentos en que ocurre un cierto porcentaje de sellado de la tubería en pozos con fracciones volumétricas de líquido elevadas (ε_l>0.5) y temperaturas entre 270°C y 305°C. El error de predicción es inferior al 3%.

Palabras clave: tiempo de sellado, escala de sílice, precipitación cinética, campo geotérmico.

http://dx.doi.org/10.18268/BSGM2024v76n1a020124

1. Introduction

Mineral precipitation poses a significant challenge in the production pipelines of geothermal wells (Mercado *et al.,* 1989). This issue primarily hinges on the chemical composition of the brine as well as the well's pressure, temperature, and mass flow conditions. Hydrogeochemical modeling serves as a valuable tool for replicating or predicting natural and technologically induced processes, including corrosion, scale formation, degassing, and more (White *et al.,* 2000; Lichti *et al.,* 2005; Bozau *et al.,* 2015). The presented predictive model aims to estimate the time required for the formation of incrustations primarily composed of minerals, specifically amorphous silica, within a pipeline. This estimation serves as one of the input data points for calculating the filling percentage. It is assumed that most of the minerals responsible for scaling originate from a brine film covering the pipe, and the volume of this film represents a proportion of the water volume circulating within the pipe during the fluid's residence time. This volume proportion is referred to as the parameter "*k*".
Dissolved silica in the brine primarily consists of silicic acid monomers. The precipitation of monomeric silica and subsequent particle formation leading to scale formation can be attributed to fluctuations in temperature and pH levels. In certain instances, these scales can disrupt the brine circulation, which serves as a heat transfer medium. Scale formation can hinder the process of brine re-injection into the reservoir and, in severe cases, compel the shutdown of power plants due to significant scaling. As noted by Durham and Walton (1999), removing scale in geothermal power plants is often a formidable challenge that can result in equipment damage over prolonged periods of operation. Consequently, this can result in an overall increase in the plant's operational expenses.

This study investigates the accumulation of amorphous silica within the Los Humeros Geothermal Field (LHGF) wells, which has been in a liquid state since the inception of depositing in the production area. Substantial reductions in temperature and pressure at these wells have led to the formation of thick crusts, particularly prevalent at shallower depths, where they rapidly evaporate (Guiza 1977; Ocampo-Díaz *et al.,* 2005). To correlate the parameters, field data from several wells of LHGF (H-01, H-13, H-15, H-16, H-17, H-17D, H-19, H24, H-32, and H-33) is used. The operating conditions and depth where fouling occurs are obtained from observational field data (Cornejo, 1996; Torres, 1995; Quijano and Torres, 1995). This data serves to simulate the behaviour of wells through equations of up-flow and heat as described in this work. The pressure and temperature conditions that determine precipitation are obtained from the results of these simulations. While the moles of the majority of minerals that precipitate per kilogramme of water are determined using speciation codes and thermodynamic precipitation (Pérez *et al.,* 2012) in conjunction with algorithms that describe the kinetic precipitation of silica in an aqueous solution (Gimón-Bastidas *et al.,* 2018).

2. Previous work

In the LHGF, various studies have been reported in the literature regarding the petrological characterization, thermal conditions, and alteration conditions in certain wells. For instance, Viggiano Guerra and Robles Camacho (1988a and b), Viggiano Guerra (1988), Prol-Ledesma and Browne (1989a, 1989b), and Martínez-Serrano and Alibert (1994), Prol-Ledesma (1998), Martínez-Serrano (2005), González-Partida *et al.* (1991a), González-Partida *et al.* (1992a), González-Partida *et al.* (1992b), González-Partida *et al.* (1993a, 1993b), González-Partida *et al.* (2022), Viggiano-Guerra *et al.* (2013), Izquierda-Montalvo *et al.* (2014), and Pandarinath *et al.* (2023) have all contributed to this body of knowledge. Similarly, several works have explored radiogenic isotopic and fluid geochemistry aspects, as documented by Arnold and González-Partida (1986a, 1986b,

http://dx.doi.org/10.18268/BSGM2024v76n1a020124

1987), Barragán *et al.* (1989), Barragán *et al.* (1991), González-Partida *et al.* (1991b), Cedillo-Rodríguez (1999), and Izquierdo-Montalvo *et al.* (2000). González-Partida *et al.* (2001), Barragán *et al.* (2002), and Yáñez-Dávila (2018) have also highlighted the high concentrations of silica in both brine and hydrothermal mineralogy.

Silicic alteration assemblages primarily consist of quartz and quartz polymorphs such as cristobalite and opal. These assemblages are typically found beneath or in proximity to sinters. Additionally, silica polymorphs tend to precipitate in the discharge pipes of hydrothermal fluids as they pass through turbines. The presence of high proportions of quartz within deep alteration assemblages (as depicted in Figure 1 and 2) signifies the distribution of deep, high-temperature argillic alteration assemblages. Truesdell (1991), Bienkowski *et al.* (2003), and Bienkowski *et al.* (2005) have previously documented the connection between deep, high-silica alterations and acidic fluids in the LHGF.

Similarly, several studies have explored the abundance of silica in relation to deep acidic supercritical fluids, often characterized by high concentrations of HCl, HF, and B in well fluids (Prol- Ledesma, 1998; Tello, 1992; Tello *et al.*, 2000; Bernard *et al.*, 2013). A notable characteristic of the LHGF is the high fraction of water vapor in brines with pH levels between 1 and 3 in deep, high-enthalpy wells (Arellano *et al.*, 2003; Izquierdo-Montalvo *et al.*, 2014). Acidic fluids in this context may result from various factors, including the exsolution of vapor from a relatively shallow hypabyssal intrusive body, deep high-temperature degassing of supercritical fluids, changes in temperature or pressure, boiling in the geothermal environment (shallow low-temperature boiling of subcritical fluids), reactivation of fractures, or oxygen leakage. Truesdell (1991) and D'Amore and Panichi (1980) have postulated the origin of these acids in the LHGF, possibly emanating from an unknown source like a magma chamber beneath the geothermal system, releasing acids such as HCl and HF into aquifers.

2.1. LOS HUMEROS GEOTHERMAL FIELD (LHGF)

LHGF is situated in Puebla, at the eastern end of the Mexican volcanic belt (19° 40' north latitude; 97° 25' west longitude), approximately 200 km from Mexico City, at an elevation of 3000 meters above sea level (as shown in Figure 1). LHGF marks the northern boundary of the Serdán-Oriental basin (Figure 1). This region is renowned for its bimodal, monogenetic volcanism, characterized by small, isolated cinder and scoria cones, large rhyolitic domes, and both rhyolitic and basaltic maars.

Exploratory studies in LHGF commenced in 1962, initiated by the Federal Electricity Commission (Mena and González, 1978; Perez, 1978; Yáñez *et al.*, 1979; Palacios and Garcìa, 1981). The first well was drilled in 1982, and electricity production began in 1990 with the commissioning of the first 5 MW generators. Subsequently, more than 40 wells have been drilled, and by 1995, there were seven units, each with a capacity of 5 MW (Quijano and Torres, 1995). Presently, the field has an installed capacity of 40 MW (Gutiérrez-Negrín, 2007).

Since the early stages of exploration and production, numerous geochemical and engineering studies have been conducted on deposits in their natural state, confirming the presence of two deposits (Arellano *et al.*, 1998). The shallower deposit, located between 1600 and 1025 meters above sea level (MASL), is characterized by a liquid phase at temperatures ranging from 300°C to 330°C and a neutral pH. In contrast, the deeper deposit, situated below 850 MASL, exhibits convective behavior, with steam typically rising from the reservoir and condensing into fluid. This deposit has a low liquid saturation and operates at temperatures between 300 °C and 400 °C (Barragán *et al.*, 2008). LHGF, with the exception of well H-01, has a high enthalpy of production, and the fluid is predominantly vapour. Heat transfer dominates the fluids in the wells, which in some cases are fed from the shallowest deposit, sometimes from the deepest, and sometimes from both (Torres, 1995).

http://dx.doi.org/10.18268/BSGM2024v76n1a020124

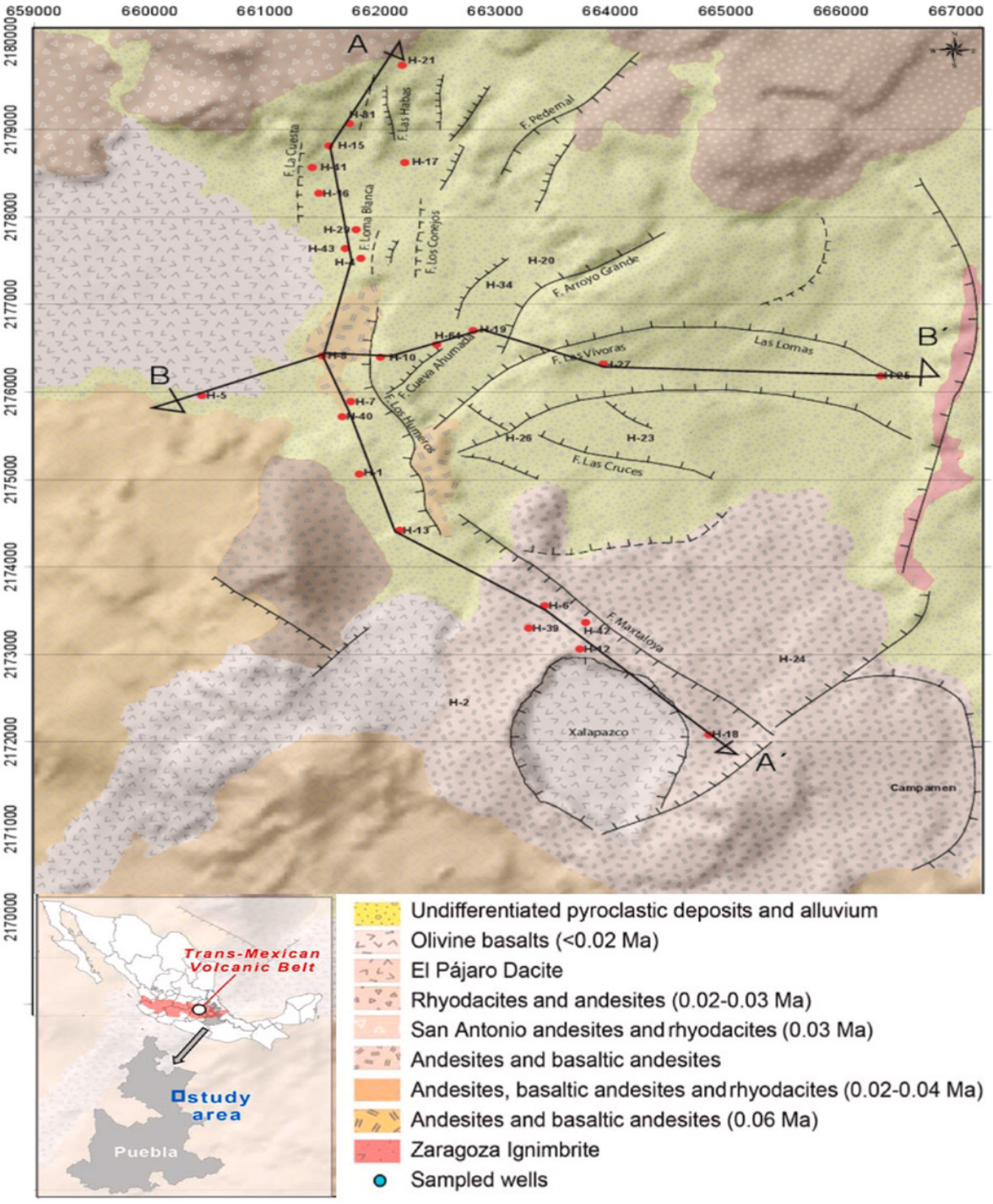

Figure 1 Local geology of the Los Humeros Geothermal Field (Puebla, central-south Mexico), showing the locations of two geological sections (A-A' and B-B') displayed in Figure 2 and the wells sampled in this study. Modified from González-Partida *et al.* 2022.

http://dx.doi.org/10.18268/BSGM2024v76n1a020124

Wells such as H-01, H-13, H-15, H-16, H-17, H-19, H-33, and H-24 (Figure 2), among others, experienced reduced production due to mineral precipitation and corrosion. In some instances, extended downtime was necessary for repairs (Cornejo, 1996; Gutiérrez and Viggiano, 1990).

The calculation of flow within wells requires the consideration of momentum transport, which includes inertia and viscous forces between fluids and between fluids and the well walls. Flows within wells are characterized by high speeds, often turbulent behavior, significant pressure gradients, and phase changes. Therefore, the calculation of flow within wells must primarily yield realistic values for density, pressure, and temperature as functions of the position along the drilling shaft. The mathematical foundations for this computational development are outlined below.

3.Methodology

3.1. ANALYTICAL APPROACH AND CALCULATIONS

In the present study, we employ the equations of mass, momentum, and energy conservation to characterize the flow within wells. There exist correlation-based and flow regime-based models that have proven effective in describing this type of flow, obviating the need for separate simulations of two- phase dynamics. We utilize a non-linear system of first-order differential equations, originally developed by Gimon-Bastidas *et al.* (2018) and integrate it with the algorithms in our study. This system simulates the kinetic dissolution and precipitation of minerals in aqueous electrolyte solutions, and it is applicable across a temperature range of 20 °C to 320 °C, pressures from 1 to 1000 bar, and ionic strengths of up to 6 mol/kg (Gimon-Bastidas *et al.*, 2018). Their numerical tool provides accurate estimations of the following: a) the types and concentrations of minerals dissolved or precipitated over time; b) the ions and cations generated and released during the kinetic dissolution or precipitation of one or more minerals in the solution (Gimon-Bastidas, *et al.* 2018).

In this article, we simulate the wells using a direct modeling approach based on the work of Gimon-Bastidas *et al.* (2018). We establish the conditions of pressure, temperature, enthalpy, and specific volume at the depth where amorphous silica filling occurs.

3.1.1. DETERMINATION OF THE TIME AT WHICH AN AMORPHOUS SILICA RING ADHERES TO THE INNER WALLS OF THE PIPELINES

As amorphous silica constitutes the predominant hydrothermal mineral phase at LHGF, silica is employed to model the incrustation processes. The precipitation of amorphous silica is most frequently encountered in pipe seals (Ocampo-Díaz *et al.*, 2005; Miranda-Herrera, 2012), and the literature extensively documents that the sealing of pipes with amorphous silica (Cornejo, 1996; Gutiérrez and Viggiano, 1990) is the primary issue facing the geothermal industry (see Figure 3). Over time, the accumulation of amorphous silica in pipelines and fluid handling equipment proves detrimental to geothermal power production. The observations made in LHGF are included in Appendix A, providing ample observational data for adjusting and validating the proposed model. Studies conducted at the Hellisheiði geothermal power plant in SW-Iceland on solution composition, saturation indices, and silica precipitations have indicated silica precipitation rates exceeding 0.35-0.75 g m^{-2} day^{-1} (Van den Heuvel *et al.*, 2018). The determination of the time required for amorphous silica scale formation relies on the following assumptions: 1) The mass flow within the pipe section remains constant; 2) The temperature, pressure, and enthalpy within this section remain consistent; 3) The pipe maintains a uniform diameter; 4) In LHGF, the predominant phase undergoing precipitation is amorphous silica; 5) Scale formation occurs regularly and uniformly; 6) Kinetically precipitated amorphous silica originates from a film whose volume represents a percentage of the

http://dx.doi.org/10.18268/BSGM2024v76n1a020124

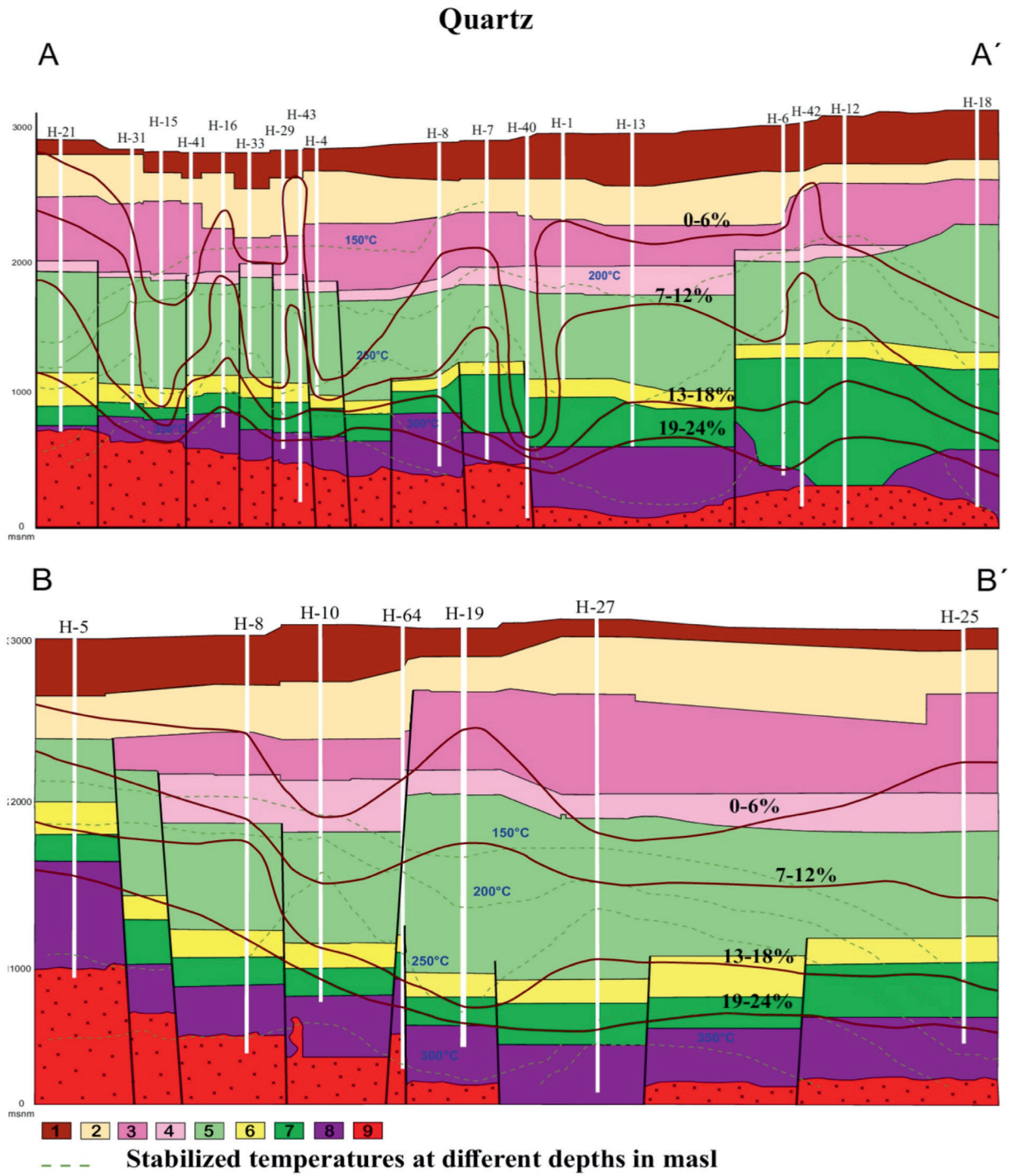

Figure 2 Los Humeros Geothermal Field sections A-A' and B-B': Distribution of quartz (in %), compared with stabilized temperatures obtained from well measurements (in ºC = dashed lines). Modified from González-Partida *et al.* 2022. Key: 1 = pumice, basalts, and andesites; 2 = lithic tuffs; 3 = ignimbrites; 4 = vitreous tuffs and ignimbrites; 5 = augite andesites; 6 = vitreous tuffs; 7 = hornblende andesites; 8 = limestones and skarn; 9 = granodiorites.

http://dx.doi.org/10.18268/BSGM2024v76n1a020124

water flowing through the pipe; 7) The brine is in equilibrium before entering the pipe section, but after entering, the fluid's temperature decreases, leading to precipitation.

3.1.2. DETERMINATION OF TOTAL MOLES OF AMORPHOUS SILICA DEPOSITED PER KILOGRAM OF WATER

Brines found in geothermal wells contain a large amount of dissolved ionized salts, primarily chlorides and sulfates, which are highly corrosive (Valdez *et al.*, 2009). The chemical analysis of the brine extracted from the Humeros wells is presented in Table 1 (Arellano *et al.*, 2001). The pH of the various brines varies, ranging from acidic (pH 5) to basic (pH 8.9), depending on the location of the well and changes over time. In the case of well H-16 brine, with a pH of 5.1, reports of corrosion exist despite having samples with a neutral pH (Gutiérrez and Viggiano, 1990). These solutions were used to determine the moles of kinetically deposited amorphous silica per kilogram of water (N_{t_0}). The characteristics of the rock in contact with the brine are presented in Table 2. The rock has a porosity of 15%.

It can take thousands of years for the interactions between brine and rock to reach a state of equilibrium with the surrounding minerals, such as potassium chloride, sodium chloride, etc., or saturation with certain salts like silica, bicarbonate, sulfide, and sulfate (Mercado *et al.*, 1989). Pérez *et al.*, (2012) utilized the temperatures listed in Table 3 and the thermodynamic equilibrium code SPCALC to determine the state of equilibrium between the brine (Table 1) and the rock (Table 2). After calculating the concentrations of species at equilibrium and the amount of thermodynamically precipitated amorphous silica, the kinetic precipitation of the amorphous silica phase was measured at a temperature 5 °C lower than the equilibrium temperature. Following the determination of kinetically precipitated moles at each of the evaluated temperatures, correlations corresponding to each well were established (Table 3).

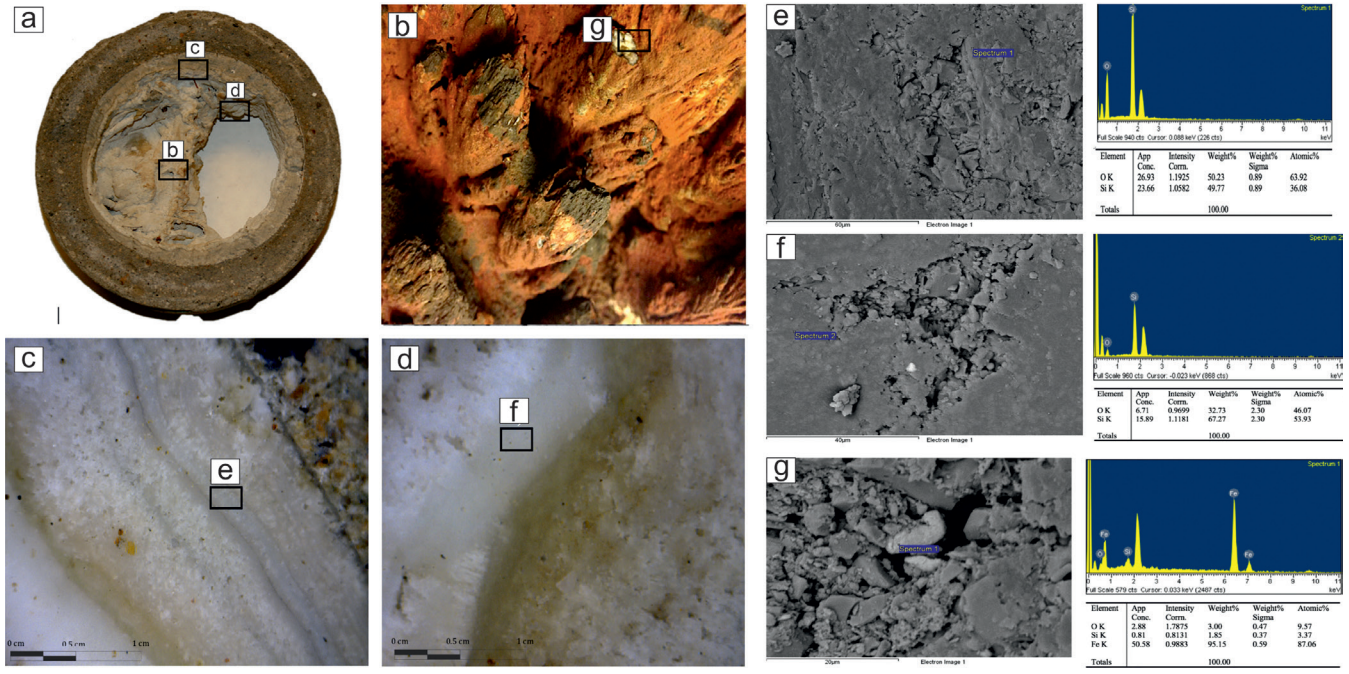

Figure 3 (a) Sealed pipe of the H-43 well at a depth of 2500 m, where the precipitation of amorphous silica can be observed (c and d), and amorphous silica with a hematite patina (b). Note the banded texture of progressive growth toward the center of the pipe. Boxes e, f, and g correspond to the areas where SEM-EDS analyses were performed, shown in microphotographs. SEM-EDS analyses reveal the compositions of the components: amorphous silica in e) and f); hematite in g) from the red patina (b).

http://dx.doi.org/10.18268/BSGM2024v76n1a020124

Table 1. Concentration of species in electrolytic aqueous solutions used in this work.

Ions in electrolyte solution (Esp.)	H-01	H-15	H-16a	H-16b	H-16c	H-17	H-19	H-20	H-30	H-31	H-32	H-33
Cl^-	180	10	268	265	99	159	1479	349	408	14	330	180
HCO_3^-	33	10	1x10-6	144	464	42	3	1.3	260	26	9.5	33
SiO_2	911	502	363	651	551	519	970	727	152	970	915	911
SO_4^{-2}	55.7	132	37	191	142	75	106	21	14	0.6	16	55.7
Na^+	180	120	43	494	586	112	340	122	112	112	107	180
K^+	27	15	9	26	32	19	45	19	14	14	21	27
Li^+	0.4	0.47	0.02	1.1	0.85	0.4	1.1	0.41	0.23	0.42	0.24	0.4
Ca^{+2}	1.7	1.2	3	2.8	0.9	0.84	4.5	23	0.8	1	5.3	1.7
Mg^{+2}	0.04	0.07	0.02	0.09	0.05	0.03	0.4	0.05	0.08	0.08	0.18	0.04
pH	7.7	5.2	5.1	7.7	8.9	7.6	5	6.8	5.3	7.7	5.7	7.7

Table 2. Amount of mineral per kg of water, in moles

Minerals	H-01	H-15	H-16	H-17	H-19	H-20	H-30	H-31	H-32	H-33
Quartz ($SiO_{2(aq)}$)	147.97	89.35	77.78	147.07	59.48	11.90	56.62	84.26	60.67	50.55
Calcite ($CaCO_3$)	89.10	78.16	67.44	39.85	0.00	0.00	58.45	0.00	0.00	0.00

Table 3. Correlations for the calculation of kinetically deposited moles of amorphous silica.

Well	T (°C)	Correlation with respect to time t (s)
H-01	280	$N_{t_0} = -7.75 \times 10^{-7} \cdot t^2 + 1.83 \times 10^{-7}$
H-13	283	$N_{t_0} = -7.18 \times 10^{-7} \cdot t^2 + 6.45 \times 10^{-5} \cdot t^2 + 1.77 \times 10^{-7}$
H-15	304	$N_{t_0} = -2.00 \times 10^{-6} \cdot t^2 + 1.545 \times 10^{-4} \cdot t^2 + 6.85 \times 10^{-8}$
H-16	305	$N_{t_0} = -1.48 \times 10^{-6} \cdot t^2 + 1.34 \times 10^{-4} \cdot t^2 + 8.02 \times 10^{-8}$
H-17	275	$N_{t_0} = -7.18 \times 10^{-7} \cdot t^2 + 6.45 \times 10^{-5} \cdot t^2 + 1.76 \times 10^{-6}$
H-19	275	$N_{t_0} = -1.56 \times 10^{-7} \cdot t^2 + 2.68 \times 10^{-5} \cdot t^2 + 1.28 \times 10^{-7}$
H-20	270	$N_{t_0} = -3.95 \times 10^{-9} \cdot t^2 + 2.42 \times 10^{-6} \cdot t^2 + 7.71 \times 10^{-9}$
H-24	289	$N_{t_0} = -2.74 \times 10^{-7} \cdot t^2 + 4.13 \times 10^{-5} \cdot t^2 + 5.18 \times 10^{-8}$
H-32	281	$N_{t_0} = -9.61 \times 10^{-8} \cdot t^2 + 2.66 \times 10^{-5} \cdot t^2 + 7.83 \times 10^{-8}$
H-33	284	$N_{t_0} = -2.74 \times 10^{-7} \cdot t^2 + 4.13 \times 10^{-5} \cdot t^2 + 5.18 \times 10^{-8}$

http://dx.doi.org/10.18268/BSGM2024v76n1a020124

3.1.3. KINETIC PARAMETER CALCULATION N_{t_0}

To determine the moles of kinetically precipitated amorphous silica (N_{t_0})over a specified time, the algorithm utilizes the following input variables: 1) The concentration of all aqueous species obtained through speciation at equilibrium, as determined by a thermodynamic speciation code (Pérez *et al.*, 2012); 2) The mass of amorphous silica that has thermodynamically precipitated, also derived from the same thermodynamic speciation; 3) The assumed specific surface area of amorphous silica, set at 1000 cm²/g; 4) Temperature; 5) The activation energy and pre-exponential factor for the dissolution or precipitation of amorphous silica, as per Palandri and Kharaka (2004).

Appendix B provides the equation defining the reaction rate for this system. The pressures used in both thermodynamic speciation and kinetic precipitation correspond to vapor pressure. Results from kinetic precipitation are presented in Figure 4 through 8.

The kinetics of amorphous silica precipitation for the various wells under study exhibit consistent behavior with increasing temperature. As temperature rises, the quantity of kinetically precipitated amorphous silica also increases. This trend is evident in Figure 4, where the ordinate axis is an order of magnitude greater than that in Figure 5.

For the H-16 well, an investigation into the effect of pH on the moles of kinetically precipitated amorphous silica was conducted. Differences in the moles of amorphous silica precipitated in solutions with varying pH levels increase at temperatures between 280 °C and 300 °C and decrease at lower (260 °C–280 °C) and higher (>300 °C) temperatures, as depicted in Figure 4 to 8. However, the sealing time for the H-16 well was determined based on the solution with a pH of 5.1, as this solution best represents the behavior of the well during the study period (Arellano *et al.*, 2001; Cornejo, 1996; Gutierrez and Viggiano, 1990).

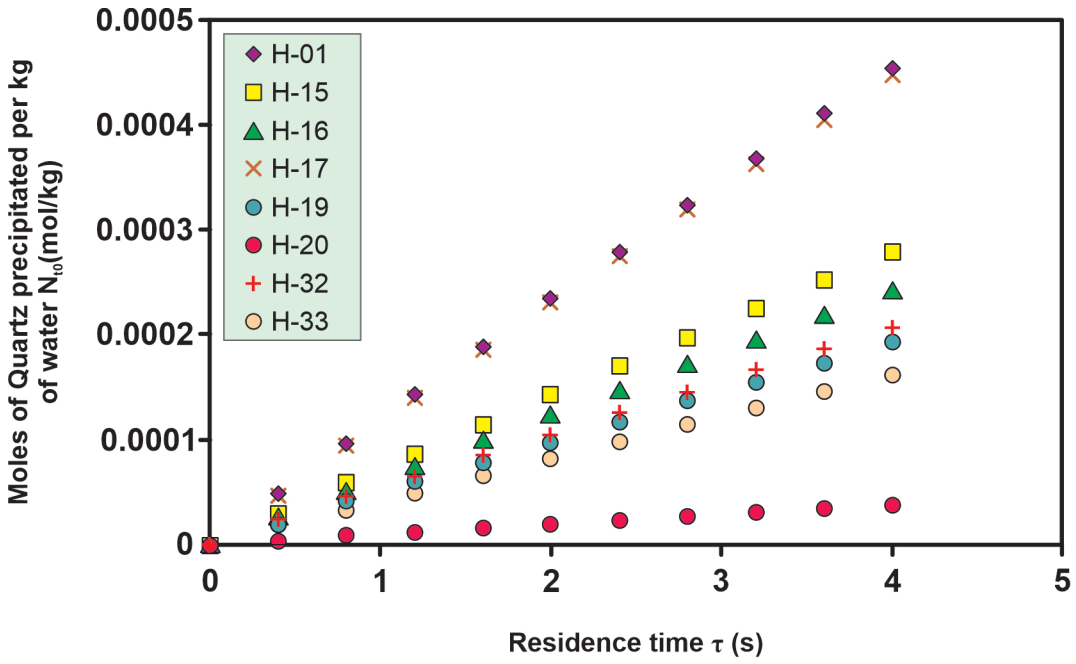

Figure 4 Kinetic precipitation of amorphous silica at a temperature of 290 ˚C for the different wells studied.

http://dx.doi.org/10.18268/BSGM2024v76n1a020124

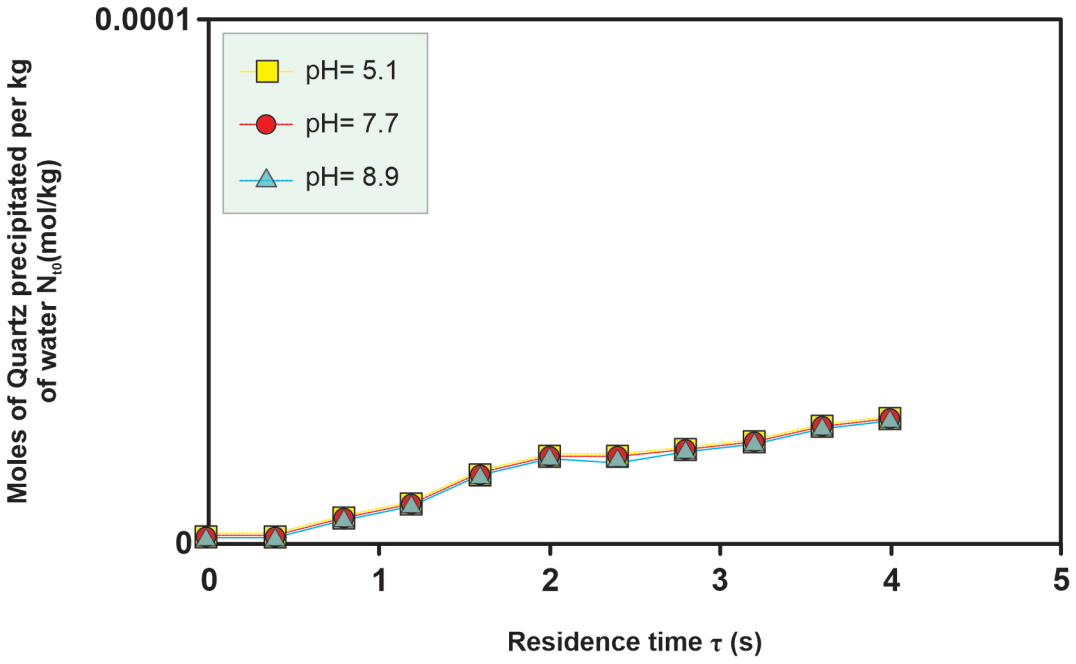

Figure 5 Kinetic precipitation of amorphous silica at a temperature of 260 ˚C for well H-16.

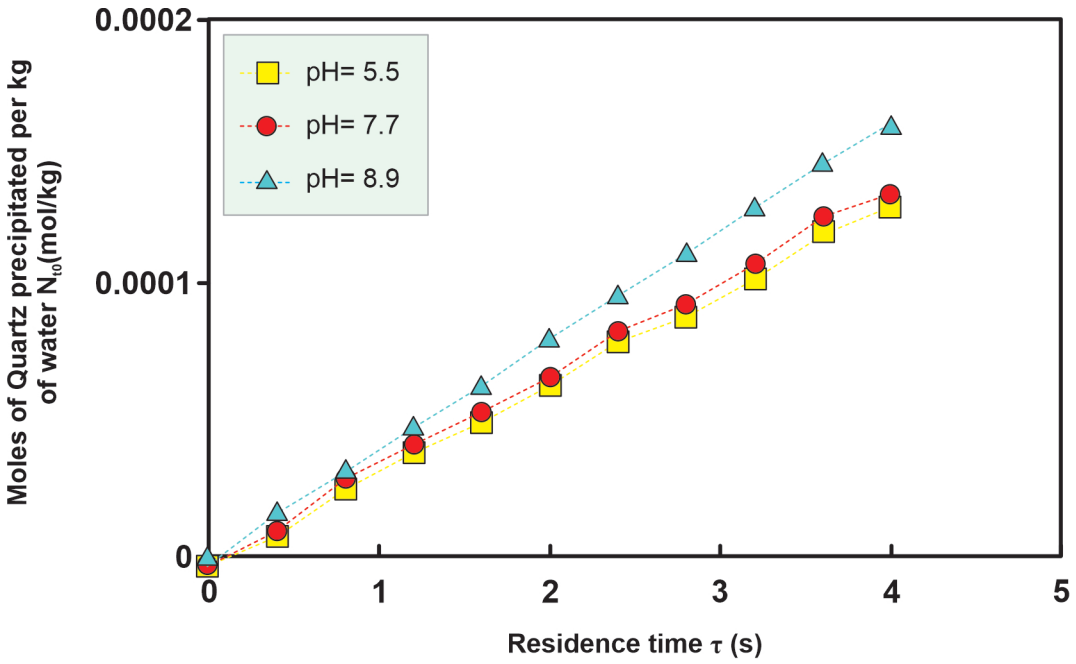

Figure 6 Kinetic precipitation of amorphous silica at a temperature of 280 ˚C for well H-16.

http://dx.doi.org/10.18268/BSGM2024v76n1a020124

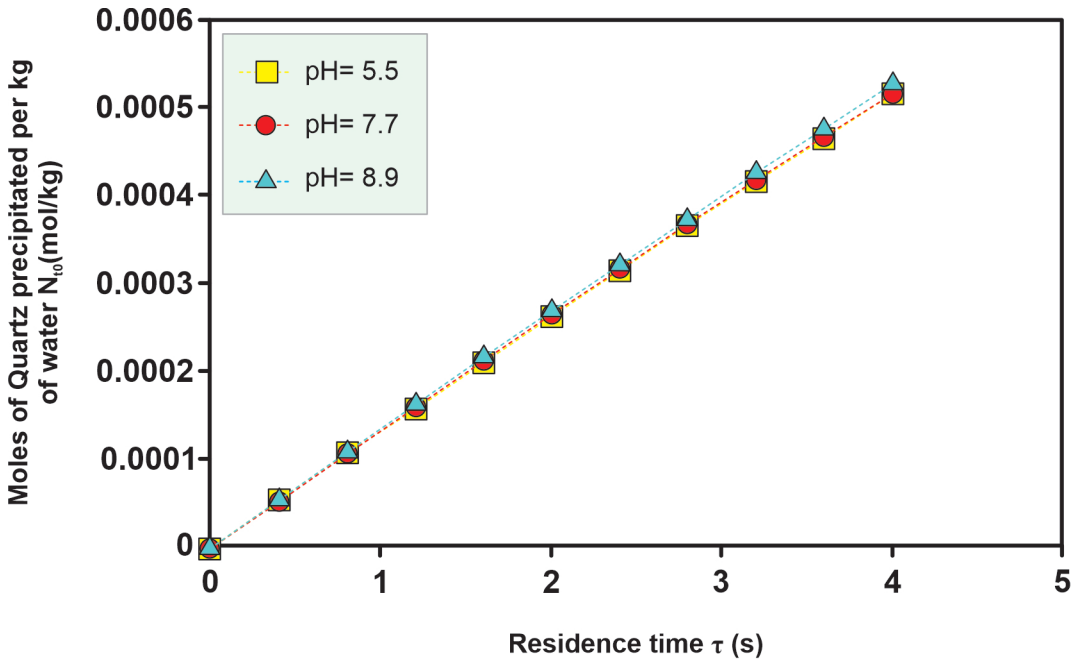

Figure 7 Kinetic precipitation of amorphous silica at a temperature of 300 ˚C for well H-16.

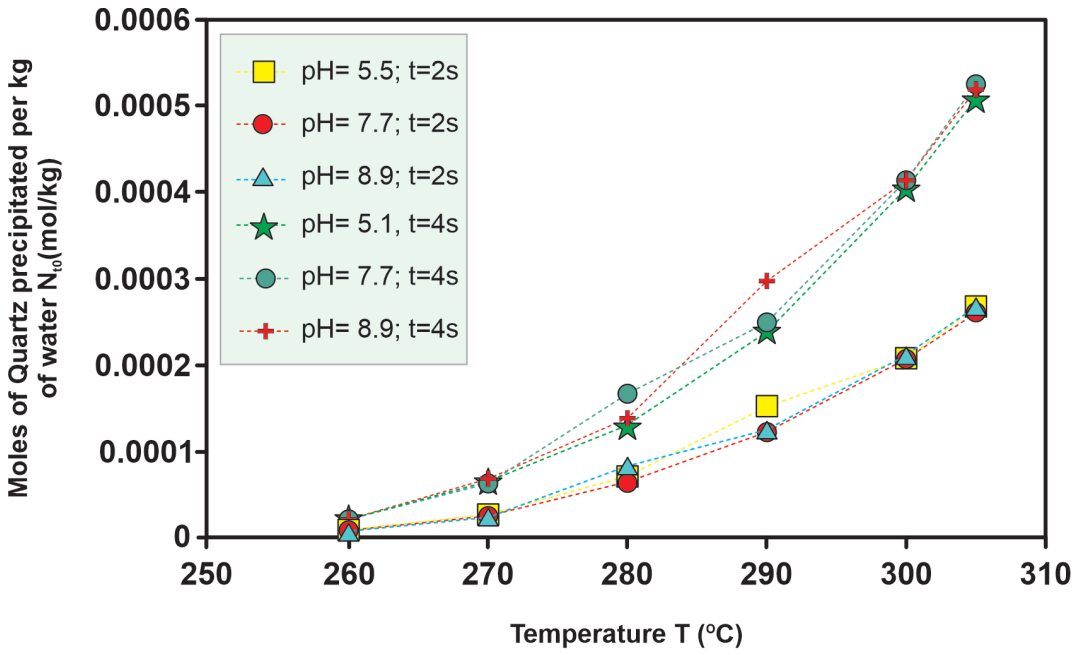

Figure 8 Kinetic precipitation of amorphous silica at different temperatures over a time of 2s and 4s for well H-16.

The algorithm summarizing the methodology used to determine the value is depicted in Figure 9. For each of the wells, a correlation was established between the moles of kinetically precipitated amorphous silica and the variables of time and temperature at the sealing point (Table 3).

Another parameter required for input into the N_{t_0} calculation algorithm (Figure 9) is the residence time (t_{res}) of the fluid in a specific section, calculated as:

$$t_{res} = {V_W}/{Q_W} \quad (1)$$

Where, V_W is the volume of water entering the pipe section under study in the first iteration and Q_W is the flow of water.

3.5. DETERMINING THE TIME AT WHICH THE AMORPHOUS SILICA RING FORMS

The two main assumptions regarding the shape of the scale and the origin of the kinetically precipitated amorphous silica are as follows: 1) The scale forms as a uniform cylindrical ring and adheres to the inner wall of the pipe (see Figure 3); 2)The amorphous silica that precipitates kinetically originates from a water film, the volume of which corresponds to a percentage of the total water present in the cylindrical section at the residence time of the water body; 3) This percentage of volume is known as the '*k*' parameter and is an adjustable parameter.

In determining the time when the amorphous silica ring forms, the following input variables are utilized: a) Pressure conditions (p), temperature (T), enthalpy (H), and mass flow rate (W) in the section of the pipe under investigation. The first three conditions are obtained from well simulations, while the mass flow rate is reported by Cornejo (1996), Quijano and Torres (1995), Torres (1995), and the Institute of Electrical Research; b) The percentage of pipe clogging (%Obt), which is either derived from literature data (Gutiérrez and Viggiano, 1990) or determined based on increased pressure in the well; c) The percentage of the total volume that constitutes the water film (k). This parameter is adjustable; d) The internal radius of the pipe (R); e) Moles of kinetically deposited amorphous silica per kilogram of water (N_{t0}); f) Water flow rate (Q_W), calculated using Equation (2); g) Liquid density (ρ_l), calculated using the function of temperature. The mass fraction of fluid vapor depends primarily on temperature, pressure, enthalpy, and is determined using IAPWS tables (2007).

$$Q_W = \frac{W.(1-X_g)}{\rho_l} \quad (2)$$

The radius obtained after ring formation (Equation 3) remains constant throughout the calculation of the ring formation time or shutter time:

$$r_{obt} = \left(1 - \frac{\%obt}{100}\right).R \quad (3)$$

Every time the cylindrical section is filled with liquid an iteration occurs. (i), at each iteration (i) The resulting radius is calculated (r_i) after the kinetic precipitation of amorphous silica using Equation 4. The algorithm for calculating training time of the amorphous silica ring, stops when:

$$r_i = R - \Delta_{r_i} \quad (4)$$

The variation of the internal radius of the pipe (Δ_{ri}- Equation 5) It is calculated from equalizing the volumes of the cylindrical ring formed by precipitated amorphous silica, calculated from the geometry of the ring (Equation 6) and the molar volume of amorphous silica (Equation 7):

$$\Delta_{r_i} = \frac{2\cdot\pi\cdot dx\cdot R - \sqrt{(2\cdot\pi\cdot dx\cdot R)^2 - 4\cdot\pi\cdot dx\cdot N_{t,i}\cdot V_{moalr}}}{2\cdot\pi\cdot dx} \quad (5)$$

Where, dx is the height of the cylindrical section, which is calculated as $dx = L/n_x$. L is the total length of the pipe and n_x is the number of subdivisions.

http://dx.doi.org/10.18268/BSGM2024v76n1a020124

$$V_i = \pi \cdot dx \cdot (R^2 - r_i^2) \quad (6)$$

$$V_i = V_{molar} \cdot N_{t,i} \quad (7)$$

Moles of amorphous silica deposited ($N_{t,i}$) at each iteration (Equation 8):

$$N_{t,i} = m_{w,i} \cdot N_{t_0} \quad (8)$$

Where N_{t0} are the moles of amorphous silica per kilogram of water deposited kinetically and $m_{w,i}$ is the body of water in the cylindrical section (Equation 9):

$$m_{w,i} = V_{w,i} \cdot \rho_l \quad (9)$$

Where $V_{w,i}$ is the volume of water that fills the cylinder at each iteration and is directly proportional to the resulting radius (r_i) squared (Equation 10):

$$V_{w,i} = \pi \cdot r_i^2 \cdot dx \cdot (1 - \varepsilon_g) \cdot k \quad (11)$$

Where ε_g is the volumetric fraction of gas and k is the percentage of the volume of liquid that forms a film of water from which amorphous silica precipitates. In each iteration the volume of water is added ($V_{w,i}$) obtained to the total volume of water passing through the cylindrical section in such a way that $r_i \leq r_{obt}$, as presented below:

$$V_{w,N} = \Sigma_{i=0}^{N} V_{w,i} \quad (12)$$

Where N is the total number of iterations, Knowing that,

$$V_{w,N} = Q_w \cdot t_{obt} \quad (13)$$

The time elapsed until the given shutter radius is reached (t_{obt}) It clears itself of the equality presented in the equation (12). The algorithm used to determine the shutter time is summarized in Figure 10.

4. Thermodynamic simulation of the wells used in the adjustment of the predictive model

Cornejo (1996) and Gutiérrez and Viggiano (1990) have provided data pertaining to the formation of amorphous silica scale in wells H-01, H-13, H-15, H-16, H-17, H-19, H-24, and H-33, all located in the LHGF in Mexico. These authors offer comprehensive information regarding the performance and operational conditions of these wells. This information encompasses values such as the enthalpy of production (H_{cab}), mass flow rate of the mixture (W), depth (L), pipe diameter (D), bottom temperatures (T_f), wellhead temperatures (T_{cab}), the location of the scale within the well, the commencement date of production, and the date of scale occurrence or well repair.

Table 4 presents a summary of the field data employed for simulating the pressure and temperature profiles of the wells used in adjusting and validating the predictive model shown in Figure 11. This table illustrates that the temperature profiles were simulated using the mathematical model of flow and heat.

4.1. MODEL ADJUSTMENT PREDICTING AMORPHOUS SILICA SCALE FORMATION TIME

The parameter '*k*' was adjusted using results obtained from simulations of six wells: H-01, H-13, H-15, H-16, H-17, and H-19. The H-01 well commenced production in 1982 (Cornejo 1996) and remained productive until 1994. In 1995, maintenance was performed on the pipe, and a seal was discovered between depths of 1295 m and 1450 m in its productive zone (Cornejo, 1996). Notably, this is the only well where the sealing zone aligns with initial conditions where the fluid was entirely in the liquid phase (see Figure 11(c)). In contrast, Wells H-13, H-15, H-16, H-17, H-17D, H-19, H-20, H-24, H-32, and H-33 had seals at shallower depths, occurring before instantaneous vaporization of the fluid and resulting in significant temperature and pressure losses within the formation

http://dx.doi.org/10.18268/BSGM2024v76n1a020124

or grid (refer to Figure 11). The Los Humeros reservoir conditions, which have governed the productive behavior since its inception, are as follows: fluids within the region of subcooled liquid near the saturation curve, low permeability, and low porosity of the system. A decrease in pressure leads to a phase change within the rock formation. Los Humeros is characterized by a low-porosity system that allows for efficient heat transfer from the rock to the fluid. Consequently, there are enthalpy variations between the wellhead and the well bottom on the order of 1200 kJ/kg. Additionally, the low permeability results in high pressure gradients between the well bottom and the wellhead (Quijano and Torres, 1995).

Thermodynamic simulations provide a close approximation to the reported values of wellhead pressure and enthalpy (Torres, 1995; Cornejo, 1996), with errors of less than 15%. Notably, Wells H-01 and H-15 (see Figure 12(b)), which draw from a single reservoir (Torres, 1995), exhibit differences in behavior. H-01, characterized by low temperatures and minimal pressure loss, experiences limited heat transfer between the fluid and the surrounding medium. Consequently, the enthalpy difference between the wellhead and the bottom is very similar, with a difference of merely 40 kJ/kg lower at the wellhead compared to the bottom. This well exhibits the highest fraction of liquid among those studied in the Humeros region.

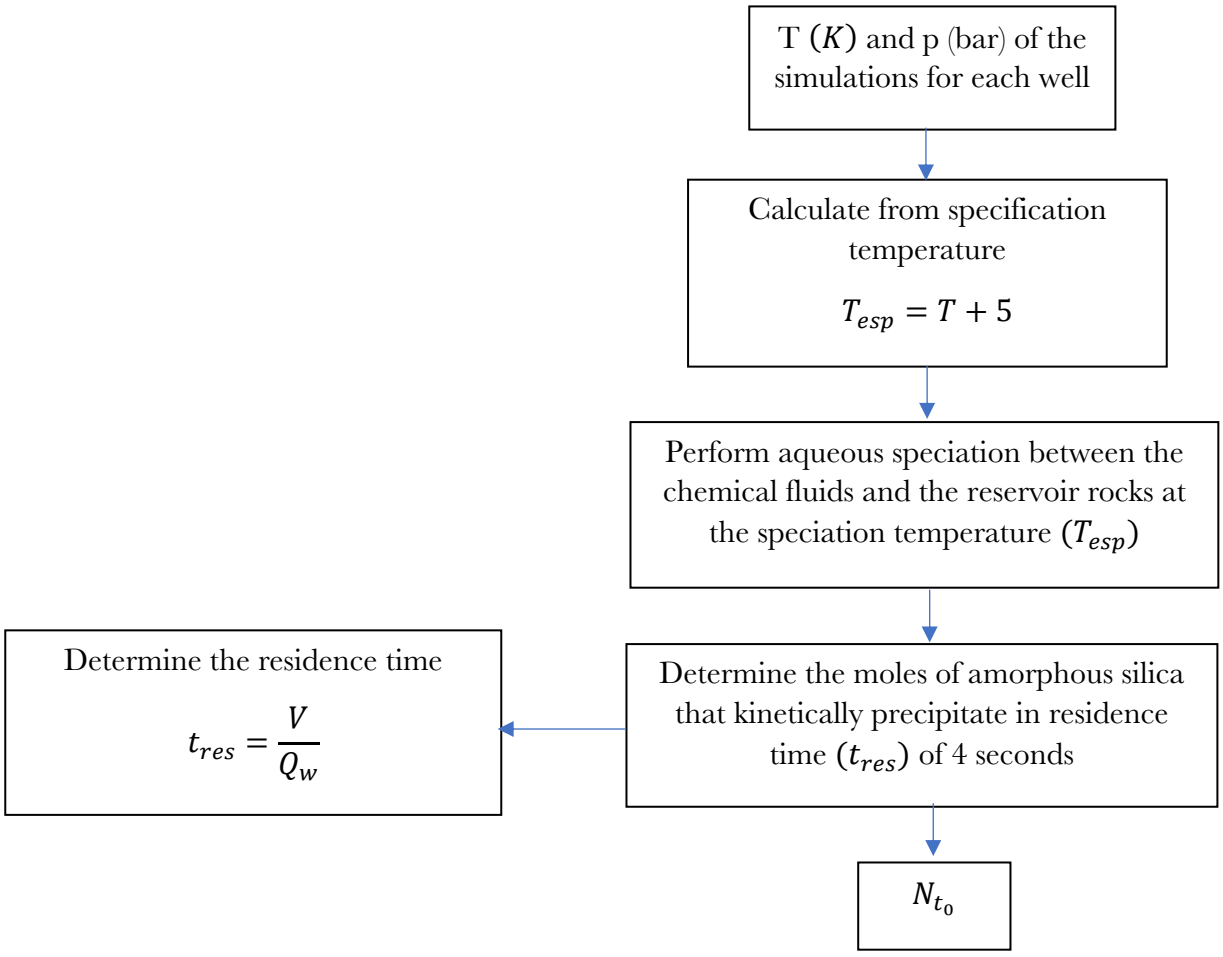

Figure 9 Algorithm used in the determination of kinetically precipitated moles of amorphous silica per kg of water. Aqueous speciation was performed for each of the chemical fluids of the wells studied in a temperature range of 260 °C to 300 °C.

http://dx.doi.org/10.18268/BSGM2024v76n1a020124

Table 4. Input data used in well simulation.

Well	D (m)	W (kg/s)	L (m)	T_f (°C)	T_{cab} (°C)	p_{cab} (bar)	H_{cab} (kJ/kg)
H-01	0.17[a]	48[a]	1450[a]	280[b]	239.86[c]	31[d]	1190[d]
H-13	0.17[a]	6.94[a]	2414[a]	315[d]	203.08[c]	15[d]	1622[d]
H-15	0.17[a]	16.94[a]	1970[a]	320[d]	257.80[c]	39[d]	2456[d]
H-16	0.17[a]	20[a]	2048[a]	318[d]	248.40[c]	38[d]	2661[d]
H-17	0.17[a]	12.5[a]	2265[a]	300[b]	218.14[c]	22[a]	2660[d]
H-17D[f]	0.24[a]	5.5[f]	1695[f]	315[e]	236.49[c]	22[e]	2664[e]
H-19	0.17[a]	12.5[a]	2292[a]	290	229.20[c]	22[d]	2640[d]
H-20	0.17[a]	10.88[f]	2252[f]	270[e]	249.87[c]	35[d]	2435[d]
H-24	0.21[a]	5.5[a]	3280[a]	300	235.82[c]	27[a]	2490[c]
H-32	0.24[f]	9.72[f]	1699[f]	307[e]	222.47[c]	25[d]	1997[d]
H-33	0.17[a]	10[a]	1600[a]	298[e]	242.24[c]	34[d]	2594[d]

[a]Cornejo 1996; [b]Quijano and Torres 1995; [c]Calculated with the mathematical simulator; [d]Torres 1995; [e]Supplied by IEE (Electrical Research Institutes); [f]Well H-17D is a well deviated from the horizontal in its repair (Cornejo 1996).

On the other hand, H-15, being the deepest well and closest to the central collapse, has higher bottom temperatures, significant contact with low-porosity rock after instantaneous vaporization, and a considerable temperature difference with the surrounding rock, favoring additional heat transfer. This results in a significantly higher fraction of steam and, consequently, a greater enthalpy difference between the wellhead and the bottom (Quijano and Torres, 1995), on the order of 1100 kJ/kg.

The enthalpy behavior and vapor fraction of Wells H-13, H-16, H-17, and H-19 (see Figure 12(a)) align with the hypothesis that these wells draw from two reservoirs (Arellano *et al.*, 1998; Torres, 1995). Vapor fraction plots reveal that the deepest reservoir, characterized by higher temperatures, experiences early boiling and high permeability, leading to a substantial pressure loss on the order of 90 bar (Quijano and Torres, 1995). This reservoir does not exhibit vapor gain beyond the instantaneous vaporization point, with vapor fractions remaining below 0.05 (see Figure 12(a) and Figure 13(c)). However, when the well is also fed by the shallower deposit, vapor gain occurs at heights near the wellhead. This behavior is not typical of dry wells with biphasic fluids since their formation (Arellano *et al.*, 2011), as observed in H-20 and H-24, which draw from a single reservoir.

The results obtained by simulating wells drawing from one or two reservoirs indicate that the algorithms developed in this study can also replicate the behavior of these wells. This expands the applicability of the mathematical model of flow and heat due to the diversity of well types in the LHGF. Another phenomenon observed aligns with Ocampo-Díaz *et al.*, (2005) descriptions. It explains that when liquid vaporization occurs, the concentration of SiO_2 increases, leading to oversaturation and precipitation of amorphous silica. This phenomenon is observed in all the studied wells in the LHGF (see Figure 11).

Figure 12(b) illustrates that the H-01 well draws from a shallow reservoir with low temperatures (ranging from 290 °C to 315 °C in the Mastayola sector (Torres, 1995)). It exhibits behavior characteristic of wells with a gas fraction (X_g) below 0.15 and minimal enthalpy variation between the formation and the wellhead. Despite drawing from a single reservoir, H-15 experiences substantial

http://dx.doi.org/10.18268/BSGM2024v76n1a020124

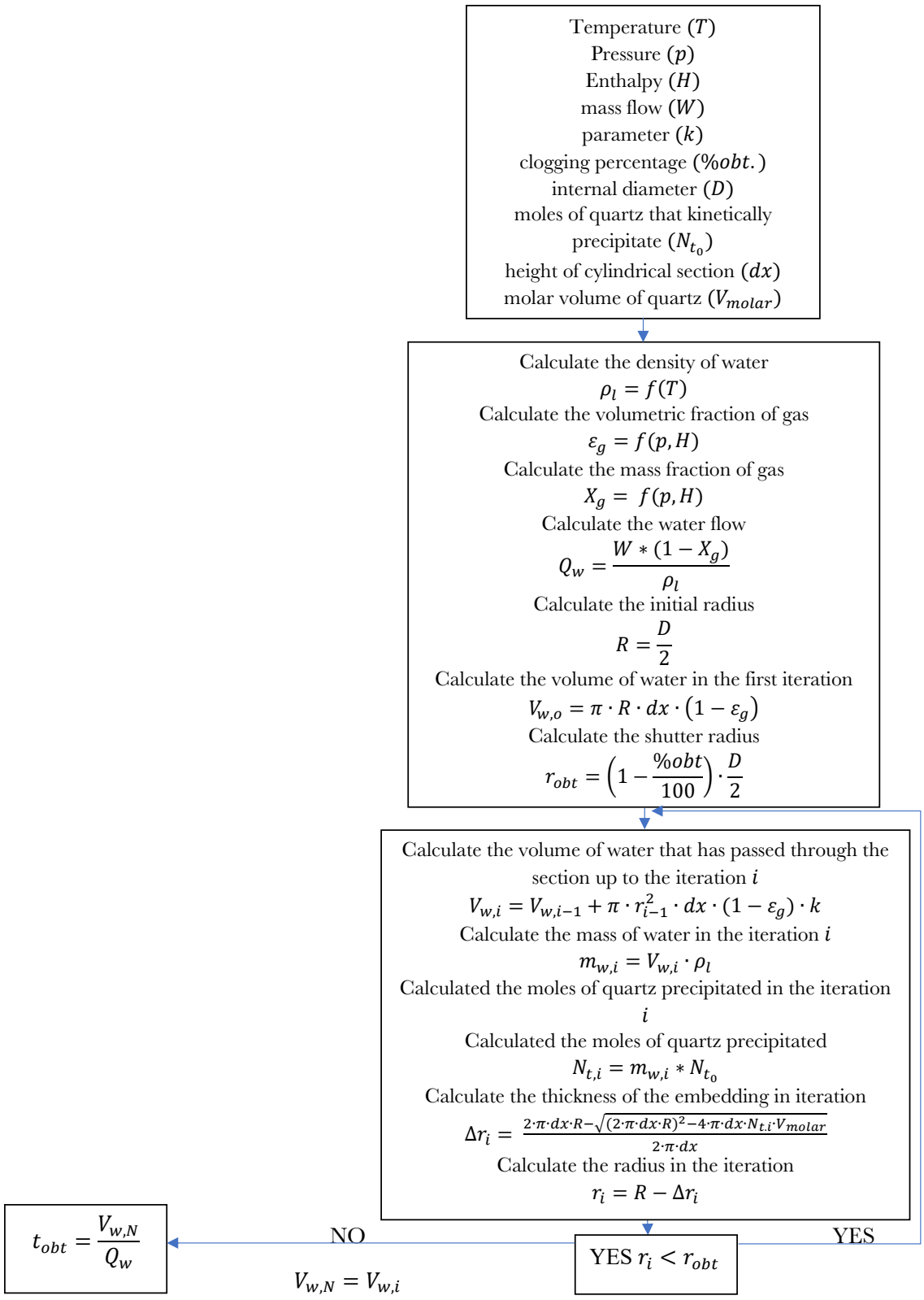

Figure 10 Determination of the time at which a certain sealing percentage is reached.

http://dx.doi.org/10.18268/BSGM2024v76n1a020124

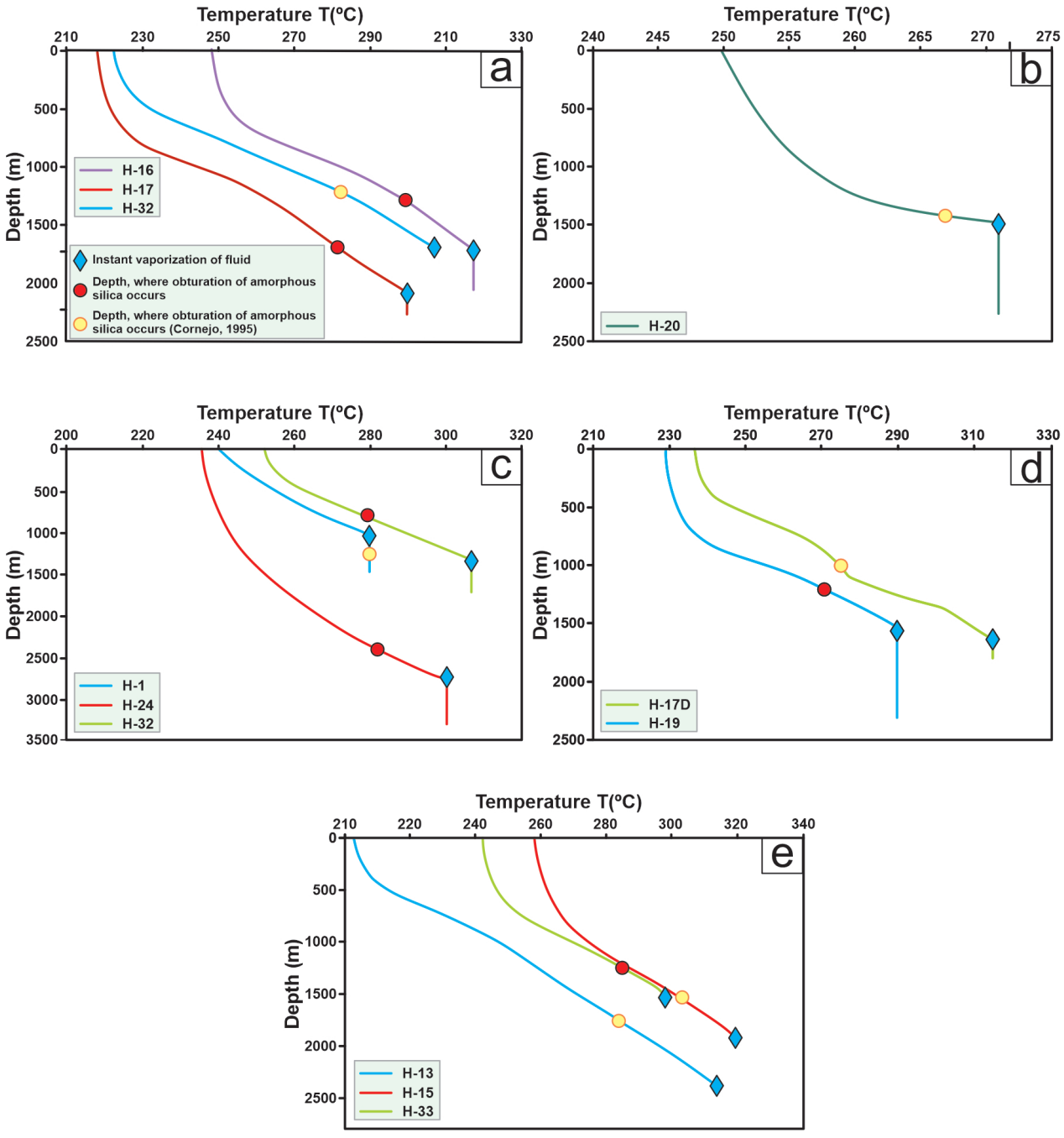

Figure 11 Temperature profiles of the LHGF studied versus the depth at which the seal is located in each of the wells. (a) Wells H-16, H-17, and H-32. (b) Well H-20. (c) Wells H-01, H-24 and H-32. (d) Wells H-17D and H-19. (e) Wells H-13, H-15, and H-33.

http://dx.doi.org/10.18268/BSGM2024v76n1a020124

vapor gain due to fluid evaporation. In Figure 11(a), the wells initially contain a significant amount of liquid in the first meters of travel, which tends to increase at heights coinciding with the feed from the shallower reservoir (between 1400 MASL and 700 MASL, according to Torres 1995). After a few meters, heat transfer promotes steam gain within the pipe, resulting in production enthalpies higher than background values, reaching up to 1200 kJ/kg.

In Figure 13(a), it becomes evident that the H-33 well draws from two deposits. Figure 13(b) demonstrates that the H-24 well is fed by a single reservoir but exhibits substantial vapor gain, particularly after the instantaneous vaporization point. Wells H-24 and H-33 were employed to validate the predictive model. Figure 13(c) illustrates that both H-17D and H-32 wells exhibit behavior akin to wells drawing from two reservoirs. Finally, Figure 13(d) shows the behavior of the H-20 well, which draws from a single reservoir. These three wells were used to estimate amorphous silica precipitation behavior under conditions similar to those used to adjust the '*k*' parameter."

The percentage of clogging of the wells used in the parameter adjustment varies between 35% and 85%, while the time needed for the amorphous silica ring to form ranges from 2 to 12 years. For each of the six wells used in the adjustment of the model, a different value was obtained for *k* (Table 5). Once these values were obtained, it was determined that the variables that have the greatest influence on the parameter are: 1) the volumetric fraction of liquid (ε_l) and 2) the product $N_{t_0} \cdot \rho_l$. From these two variables, a correlation was constructed (Equation 12) that predicts the value of the parameter, knowing the volumetric fraction of the liquid, the density of the liquid, and the moles of amorphous silica that precipitate kinetically per kilogramme of water. Table 6 presents the results of the adjustment, and it can be seen that the time needed for the scale to form is predicted with errors less than 3%.

$$k = 77.45 - 92.99 \cdot \varepsilon_l - 4169 \cdot N_{t_0} \cdot \rho_l + 18.06 \cdot {\varepsilon_l}^2 + 3693 \cdot \varepsilon_l \cdot N_{t_0} \cdot \rho_l + 27810\left(N_{t_0} \cdot \rho_l\right)^2 \quad (12)$$

The time in which a certain percentage of seal is reached increases as the percentage of seal increases (Figure 14). In some wells, scale forms more quickly than in others; for example, wells H-15, H-16, H-17, and H-19 seem to reach a certain percentage of seal faster than wells H-01 and H-13. This has to do with the characteristics of each well. The results of this predictive model are validated by evaluating its performance by simulating wells H-24 and H-33, for which operating time data are available.

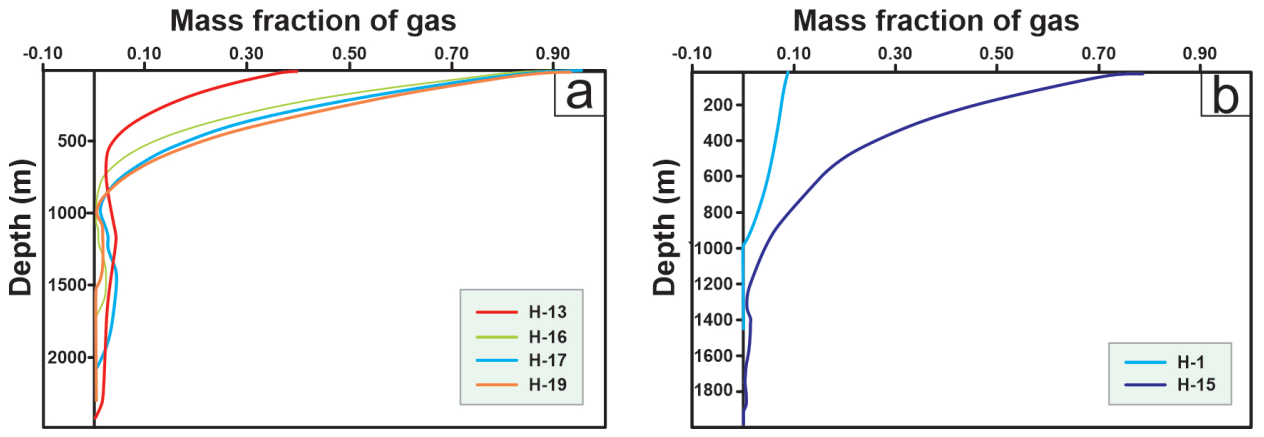

Figure 12 Gas fraction profiles of the wells in the LHGF. (a) Wells fed from two reservoirs. (b) Wells fed by a single reservoir.

http://dx.doi.org/10.18268/BSGM2024v76n1a020124

Table 5. Operating conditions at the height where precipitation scale of the amorphous silica phase is formed.

Well	Temperature in the section (°C)	Pressure on the section (bar)	Enthalpy in the section (kJ/kg)	N_{t_0} (mol)	Height where the shutter is located (m)	% Obt	k (%)	Time to reach % Obt - Experimental (years)
H-01	279.99[a]	83.43[a]	1235.53[a]	2.54x10-05	1295[b]	85	0.18	12.06[b]
H-13	283.00[a]	67.12[a]	1283.39[a]	1.19 x10-04	1735[b]	85	0.47	6.97[b]
H-15	304.17[a]	91.04[a]	1383.45[a]	1.49 x10-04	1580[b]	85	0.26	4.43[b]
H-16	305.22[a]	92.38[a]	1400.21[a]	9.30 x10-05	1418[c]	46[c]	0.26	4.05[c]
H-17	275.49[a]	59.91[a]	1273.15[a]	5.08 x10-05	1550[b]	85	1.09	3.99[b]
H-19	275.39[a]	59.87[a]	1235.91[a]	2.99 x10-05	1280[b]	35	2.30	1.85[b]

[a] Calculated with the mathematical simulator; [b] Cornejo 1996; [c] Gutiérrez and Viggiano 1990.

Table 6. Predictive model tuning, parameter k.

Well	% Obt.	k (%)	ε_l	ρ_l (kg/cm^3)	$N_{t_0} \cdot \rho_l$ (mol/m^3)	Time to reach % Obt Experimental (days)	Time to reach % Obt Model (days)	Relative error (%)
H-01	85	0.18	1.00[a]	750.29[a]	0.019102176	4380	4403	0.52
H-13	85	0.47	0.69[a]	744.90[a]	0.088794392	2525	2542	0.67
H-15	85	0.26	0.86[a]	703.40[a]	0.105264679	1610	1618	0.49
H-16	46[b]	0.26	0.78[a]	701.15[a]	0.065240763	1460	1478	1.23
H-17	85	1.09	0.50[a]	758.16[a]	0.038521132	1460	1454	-0.41
H-19	35	2.30	0.73[a]	758.24[a]	0.022682937	660	675	2.27

[a] Calculated with the mathematical simulator; [b] Cornejo 1996; [c] Gutiérrez and Viggiano 1990.

Table 7. Performance of the predictive model in the wells used for its validation.

Well	Temperature (°C)	N_{t_0} (mol)	Diameter (m)	W (kg/s)	% Obt	k	Time to reach %Obt Exp. (days)	Time to reach %Obt Model (days)	Relative error (%)
H-24	288.96[a]	1.3x10-4	0.21[b]	5.5[b]	85	0.72[c]	2735[b]	2663	-2.63
H-33	284.17[a]	5.9x10-5	0.17[b]	10[b]	85	0.91[c]	1855[b]	1809	-2.47

[a] Calculated with the mathematical simulator; [b]Cornejo 1996; [c]Calculated by Equation 12.

Table 8. Projections of wells for which seal time information is not available.

Well	Temperature (°C)	N_{t_0} (mol)	Diameter (m)	W (kg/s)	% Obt	k	Time to reach %Obt Model (days)
H-17D	278.61[a]	9.15x10-5	0.24[b]	5.5[c]	85[c]	0.15[d]	24983
H-20	270.89[a]	4.20x10-6	0.17[b]	10.88[b]	85	1.58[d]	13402
H-32	268[a]	8.05x10-5	0.24[b]	9.72[b]	85	0.15[d]	15708

[a]Calculated with the mathematical simulator; [b]Cornejo 1996; [c]Aragón and Gonzales 2014; [d]Calculated by Equation 12.

http://dx.doi.org/10.18268/BSGM2024v76n1a020124

4.2. VALIDATION OF THE MODEL THAT PREDICTS THE FORMATION TIME OF AMORPHOUS SILICA SCALE

Cornejo (1996) provides information on the initiation and operational periods of wells H-24 and H-33. Both wells underwent direct modeling simulations, and the errors in predicting the time when scale formation occurs for H-24 and H-33 wells (as presented in Table 8) are below 3%. This demonstrates that the predictive model is accurate and effectively replicates the time at which well sealing occurs under the following conditions: 1) Temperatures within the range of 270°C to 305°C; 2) Enthalpies ranging from 1187 to 1400 kJ/kg; 3) Volumetric fractions of liquid (ε_l>0.5) between 0.5 and 0.99; As seen in previous cases, with the passage of time, the percentage of sealing within the pipes increases (as illustrated in Figure 15). Additionally, we selected three wells that have not experienced closure due to sealing issues, but share temperature conditions similar to those of the wells under investigation. The results are summarized in Table 7, where the estimated sealing times range from 36 to 68 years under these conditions. This estimate serves as an additional validation of the model, as, at the time of this study, none of the wells had reached the sealing time predicted by the model (refer to Figure 16). H- 17D has been in operation since 1993 following repairs (Cornejo 1996), H-20 has been operational since 1988, and H-32 since 1989 (Torres 1995).

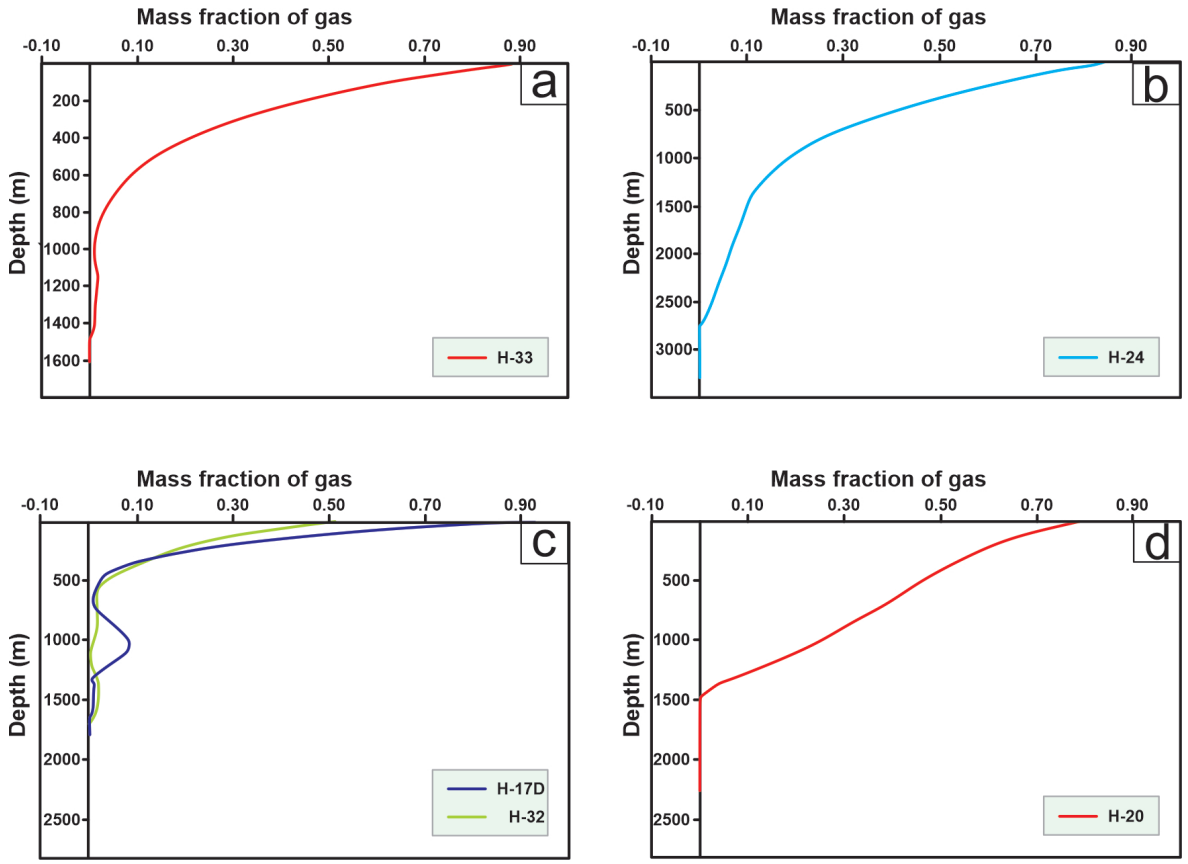

Figure 13 Profiles of the gas mass fraction of the wells in the LHGF. (a) Well H-33, fed by two reservoirs, used for model adjustment. (b) Well H-24, fed by a reservoir, used for model adjustment. (c) Wells H-17D and H-32, fed by two reservoirs, used to estimate operating time. (d) Well H-20, fed by a reservoir, used to estimate operating time.

http://dx.doi.org/10.18268/BSGM2024v76n1a020124

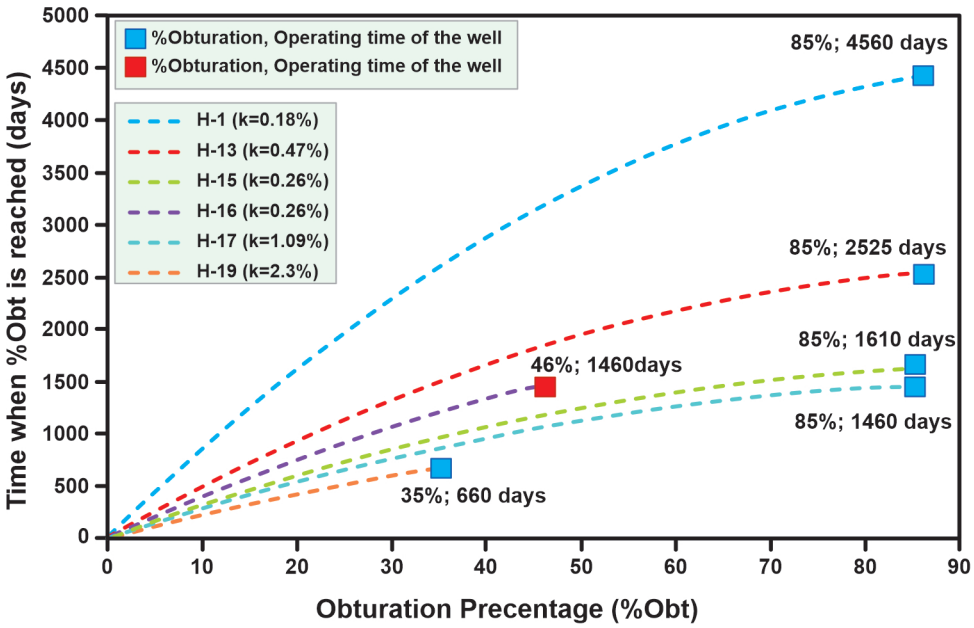

Figure 14 Variation in the percentage of plugging over time for the wells used in the adjustment of parameter k.

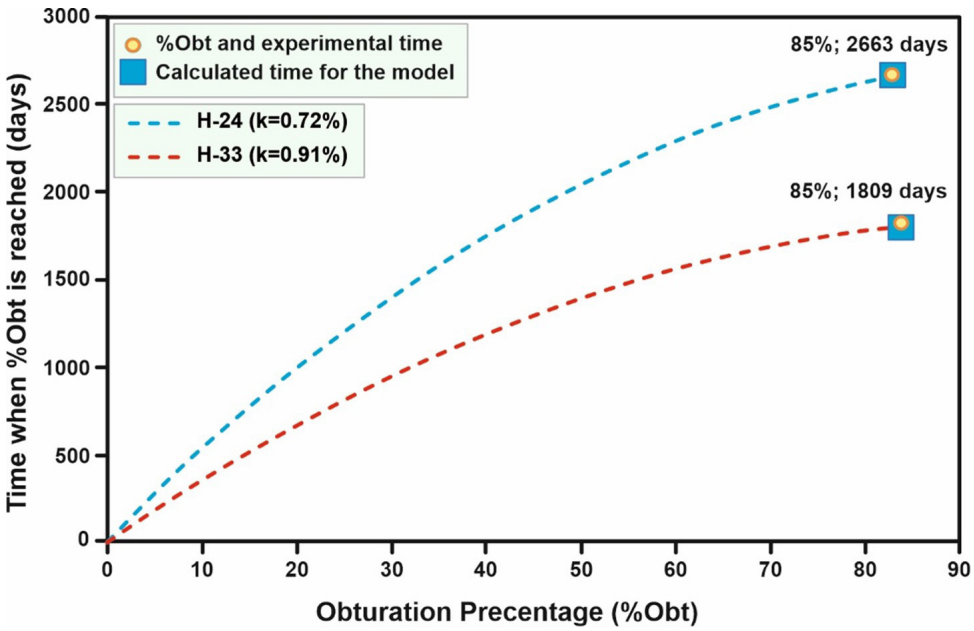

Figure 15 Changes in the percentages of sealing over time for the wells used in the validation of the correlation used to determine the parameter k.

http://dx.doi.org/10.18268/BSGM2024v76n1a020124

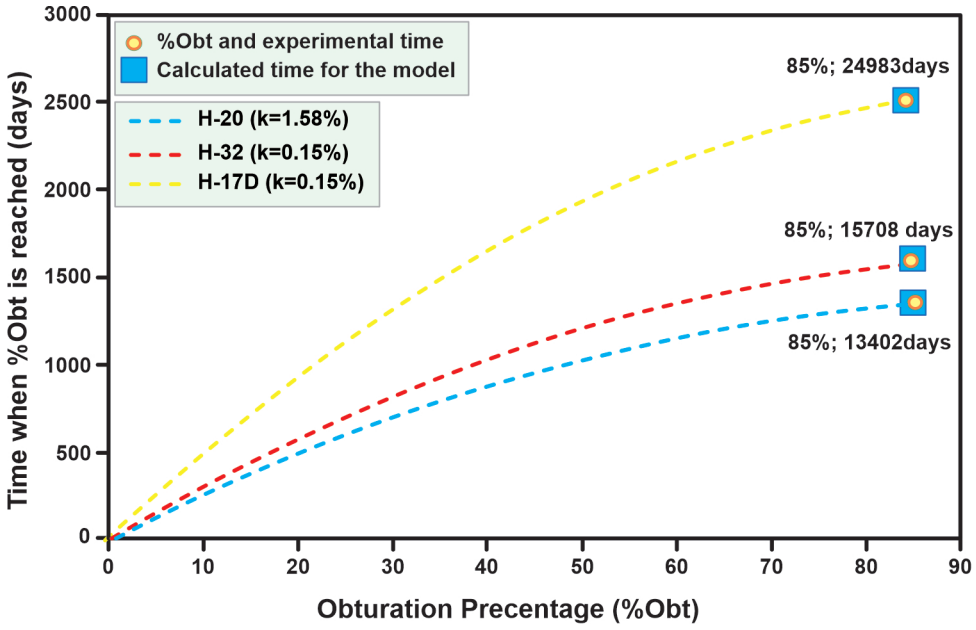

Figure 16 Wells used to verify the model through sealing time projections.

5. Limitations

The proposed model for predicting amorphous silica obstruction in geothermal wells demonstrates promising potential within its defined scope. While its applicability may be more tailored to environments resembling Los Humeros, its specificity ensures a focused and accurate analysis in such contexts. The model's dependence on precise input parameters, although a limitation, underscores the importance of meticulous data collection for optimal performance. Seeing that the model only works with two-phase flow as a possible limitation makes it clear that we need to learn more about it and change it to work with situations where the fluids or flow patterns are different. Focusing on amorphous silica makes the model easier to use and helps with specific insights, even though it makes the mechanisms of scale formation simpler. Continuous efforts in ongoing research and validation endeavors are integral, serving as proactive measures to refine the model and extend its utility to a broader array of geothermal fields. The model's limitations, therefore, serve as stepping stones for improvement and evolution, contributing to the continuous advancement of predictive capabilities in geothermal well management.

6. Conclusion

The model developed in this study accurately predicts the point in time when pipe sealing reaches a certain percentage in wells. This prediction is reliable when volumetric fractions of liquid are high ($\varepsilon_l > 5$) and when temperatures remain within the range of 270 °C to 305 °C, with stable temperature, pressure, and enthalpy profiles over their production periods.

To enhance the performance of this model, we propose incorporating simulations that account for changes in pipe diameter due to amorphous silica accumulation. These changes influence temperature, pressure, and enthalpy at the depth where sealing occurs.

http://dx.doi.org/10.18268/BSGM2024v76n1a020124

Our algorithm is highly sensitive to variations in mass flow and diameter, which have a significant impact on residence time calculations. Therefore, we recommend expanding the number of samples used in adjusting the *'k'* parameter and introducing a term that considers the fluid's residence time in the pipe section.

In the case of well H-16, it was observed that the moles of amorphous silica precipitate more as the temperature increases, and differences were noted among solutions with pH values of 5.1, 7.7, and 8.9 at temperatures ranging between 280 °C and 300 °C. As the kinetic precipitation of amorphous silica is proportional to the residence time (the time it takes to fill the pipe), wider pipes and lower mass flows, such as those in Humeros, result in more significant amorphous silica deposition due to longer filling times.

Thermodynamic simulations were generated from adjustments of flow and heat models, producing accurate pressure and enthalpy profiles with errors between 1% and 15%. These simulations revealed that wells H-13, H-16, H-17, and H-19 draw from two reservoirs.

Wells fed from two reservoirs often encounter sealing and corrosion issues, leading to the maintenance-related closure of these wells. Upon reopening, these wells typically recover 75% of their production. Therefore, it is advisable to ensure that wells operate with a single reservoir feed whenever possible, as amorphous silica precipitates more readily in such wells, as observed in the behavior of wells H-13, H-16, H-17, and H-19.

The results obtained from simulating a diverse range of wells in the LHGF confirm the reliability and accuracy of the predictive precipitation model, with relative errors below 3%.

Early utilization of this type of model for characterizing production fields, in conjunction with traditional approaches, can positively influence the improvement of well construction characteristics and the implementation of preventive measures to mitigate mineral precipitation-induced clogging.

Declaration of competing interest

The authors declare that they have no known competing financial interests or personal relationships that could have appeared to influence the work reported in this paper.

Acknowledgment

This research was supported by the GEMex Project: Mexico-Europe Cooperation for the investigation of enhanced geothermal systems and super-hot geothermal systems, CALL S0019-2015-4, funded by the Energy Sustainability Fund, CONACYT-SENER, Project No. 268074, PT. 4.8 and 6.2. We express our gratitude for the financial support provided by CONAHCyT for the Project, CF-2023-G- 490, titled 'Determinación Geoquimiométrica de Tierras Raras en Matrices Geotérmicas de Interacción Roca-Fluido para la Evaluación Teórica-Experimental de Estructuras Moleculares y Patrones Multivariados de Fraccionamiento y Movilidad.' We also acknowledge post-doctorate fellowships awarded to SM and JM by DGAPA-UNAM and CONACYT, respectively.

Authors Contribution

All authors contributed to the study conception and design. Material preparation, data collection and analysis were performed by Sumit Mishra, Eduardo González-Partida, Sanjeet K. Verma, Kailasa Pandarinath, R. Pérez-Rodríguez, Joseph Madondo, and Antoni Camprubí. The first draft of the manuscript was written by Sumit Mishra, Eduardo González-Partida and all authors commented on previous versions of the manuscript. All authors read and approved the final manuscript.

Conflicts of Interest

The authors declare no potential conflict of interest.

http://dx.doi.org/10.18268/BSGM2024v76n1a020124

Handling editor

Francisco J. Vega.

Data Availability Statement

The data that support the findings of this study are available from the corresponding author upon reasonable request.

References

Aragón-Aguilar, A., Gonzales, E., 2014, Síntesis de Alteraciones Hidrotermales Humeros: Instituto de Investigaciones Eléctricas, Reporte Técnico, 88.

Arellano, V.M., Barragán, R.M., Aragón, A., Rodríguez, M.H., Pérez, A., 2011, The Cerro Prieto IV (México) geothermal reservoir: Pre-exploitation thermodynamic conditions and main processes related to exploitation (2000–2005): Geothermics, 40(3), 190–198. https://doi.org/10.1016/j.geothermics.2011.06.001

Arellano, V.M., Izquierdo, G., Aragón, A., Barragán, R.M., García, A., Pizano, A., 2001, Distribución de presión inicial en el campo geotérmico de Los Humeros, Puebla, México: Ingeniería Hidráulica en México, 16(3), 75–84.

Arellano, V.M., García, A., Barragán R.M., Izquierdo, G., Aragón, A., Nieva, D., 2003, An updated conceptual model of the Los Humeros geothermal reservoir (Mexico): Journal of Volcanology and Geothermal Research, 124(1-2), 67–88. https://doi.org/10.1016/S0377-0273(03)00045-3

Arellano, V.M., García, R.M., Barragán, G., Izquierdo, Aragón A., Nieva, D., Portugal, E., Torres, I., 1998, Desarrollo de un modelo básico actualizado del yacimiento geotérmico de Los Humeros, Puebla: Cuernavaca, México, Instituto de Investigaciones Eléctricas, Informe interno.

Arnold, M., González-Partida, E., 1986a, Capacités oxidantes d'un fluide hydrothermale en ´ebullition: Comptes Rendus de l'Académie des Sciences de Paris, 303, 817–821.

Arnold, M., González-Partida, E., 1986b, Le système sulfate-sulfure; prouves d'un equilibre chimique a 300 ºC: consequences géoquimiques: Comptes Rendus de l'Acad´emie des Sciences de Paris, 303, 1097–1099

Arnold, M., González-Partida, E., 1987, Le système hydrothermal actuel de Los Humeros, Mexique: Etat du systeme SO4-SH2 à 300 ºC, origine du soufre et phenomenes d'oxydation associés a l' ébullition du fluide ascendant: Miner Deposita, 2(2), 90–98. https://doi.org/10.1007/BF00204685

Barragán, R., Arellanos, G., Armenta, F., Aguado, T., 2008, Cambios químicos en fluidos de pozos del campo geotérmico de Los Humeros: Evidencia de recarga profunda: Geotermia. Revista Mexicana de Geoenergía, 21(2), 11–20.

Barragán, R.M., Arellano, V.M., Portugal, E., García, A., Tovar, R., 2002, Gas geochemistry in modelling geothermal reservoirs: Geofísica Internacional, 41(3), 243–254. https://doi.org/10.22201/igeof.00167169p.2002.41.3.338

Barragán, R.M., Nieva, D., González-Partida, E., López, M. J.M., 1989, Comportamiento químico del fluido del pozo H-16 en el Geotérmico de Los Humeros: Unión Geofísica Mexicana, 9(4), 245–252.

Barragán, R.M., Nieva, D., Santoyo, E., González-Partida, E., Verma, M., López, J., 1991, Geoquímica de fluidos del campo geotérmico de Los Humeros (México): Geotermia. Revista Mexicana de Geoenergía, 7(1), 23–47.

Bernard, R., Taran, Y., Pennisi, M., Tello, E., Ramirez, A., 2013, Chloride and boron behavior in fluids of Los Humeros geothermal field (Mexico): a model based on the existence of deep acid brine: Applied Geochemistry, 26(12), 2064–2073. https://doi.org/10.1016/j.apgeochem.2011.07.004

Bienkowski, R., Torres-Alvarado, I.S. and Hinderer, M., 2003, Genese hochsaurer Fluide im Geothermalfeld von Los Humeros, Zentral-Mexiko. MSc Thesis, Institut für Angewandte Geowissenschaften, Technische Universität Darm- stadt, Diplomarbeit, 89 p.

Bienkowski, R., Torres-Alvarado, S., Hinderer, M., 2005, Geochemical modeling of acid fluids in Los Humeros geothermal field, Mexico, in Proceedings World Geothermal Congress 2005: Antalya, Turkey, 24–29.

Bozau, E., Steffen, H., Van Berk, W., 2015, Hydrogeochemical modelling of corrosion effects and barite scaling in deep geothermal wells of the North German Basin using PHREEQC and PHAST: Geothermics, 53, 540–547. https://doi.org/10.1016/j.geothermics.2014.10.002

Campos, J.O., Garduño, V.H., 1987, The shallow structure of Los Humeros and Las Derrumbadas geothermal fields, México: Geothermics, 16(5-6), 539–554. https://doi.org/10.1016/0375-6505(87)90038-1

Carrasco-Núñez, G., Gomez-Tuena, A., Lozano, L., 1997, Geologic map of Cerro Grande volcano and surrounding area, Central Mexico: Geological Society of America, Map and Chart Series, MCH 81 (10).

Castro, S.C., 1996, Well repairing at the Los Humeros, Mexico, geothermal field (No.

CONF-960913-): Geothermal Resources Council, Davis, CA (United States), 20, 567–574.

Cedillo-Rodríguez, F., 1999, Modelo hidrogeológico de los yacimientos geotérmicos de Los Humeros, Pue., Mexico: Geotermia. Revista Mexicana de Geoenergía, 15(3), 159–170.

Cornejo, S., 1996, Well Repairing at the Los Humeros, Mexico, Geothermal Field: Geothermal Resource Council Transactions, 20, 567-574.

D'Amore, F., Panichi C., 1980, Evaluation of deep temperature of hydrothermal systems by new gas geothermometer: Geochimica et Cosmochimica Acta. Cosmochi, 44(3), 549–556. https://doi.org/10.1016/0016-7037(80)90051-4

Durham, B., Walton, A., 1999, Membrane pretreatment of reverse osmosis: long-term experience on difficult waters: Desalination, 122(2-3), 157–70. https://doi.org/10.1016/S0011-9164(99)00037-5

Ferriz, H., Mahood, G.A., 1984, Eruption rates and compositional trends at Los Humeros volcanic center, Puebla, Mexico: Journal of Geophysical Research: Solid Earth, 89(B10), 8511–8524. https://doi.org/10.1029/JB089iB10p08511

Gimón-Bastidas, R.J., Pérez-Rodríguez, R.J., González-Partida, E., 2018, Desarrollo computacional de las ecuaciones cinéticas para la disolución/precipitación de minerales en fluidos acuosos: Boletín de la Sociedad Geológica Mexicana, 70(3), 567–590. https://doi.org/10.18268/bsgm2018v70n3a1

Gómez-Tuena, A., Orozco-Esquivel, M., Ferrari, L., 2005, Petrogénesis ígnea de la faja volcánica transmexicana: Boletín de la Sociedad Geológica Mexicana, 57(3), 227–283. https://doi.org/10.18268/bsgm2005v57n3a2

González-Partida, E., Camprubí, A., López-Hernández, A., Santoyo, E., Izquierdo-Montalvo, G., Pandarinath, K., Yáñez-Dávila, D., González-Ruiz, L.E., González-Ruiz, D., Díaz-Carreño, E., Juárez-Hilarios, E., 2022, Distribution of hypogene alteration and fluid evolution in the Los Humeros Geothermal Field (Puebla, Mexico): Multiple sourced fluids, interrelations, and processes in a superhot system: Applied Geochemistry, 136, 105–159.

González-Partida, E., Tello-Hinojosa, E., Verma, M.P., 2001, Interacción agua geotérmica-manantiales en el campo geotérmico de Los Humeros, Puebla, México: Tecnología y Ciencias del Agua, 16(2), 185–194.

González-Partida, E., Barragán, R., Nieva, G.D., 1993a, Las especies carbónicas del fluido

geotérmico de Los Humeros, Puebla, México: Geotermia. Revista Mexicana de Geoenergía, 9, 205–218.

González-Partida, E., Barragán, R.M., Nieva, D., Quijano, J.L., López, J.M., Gutiérrez, P.H., 1991a, Estudio de inclusiones fluidas en cuatro pozos del campo geotérmico de Los Humeros, Puebla: Geotermia. Revista Mexicana de Geoenergía, 7(2), 201–229.

González-Partida, E., Barragán, R.M., Torres, R., 1991b, Comportamiento de la salmuera geotérmica en diagramas de estabilidad: aplicación en el campo de los Humeros, Pue.: Actas de la Facultad de Ciencias de la Tierra, Universidad Autónoma de Nuevo León, 6, 21–126.

González-Partida, E., Barragán, R.M., Nieva, G.D., 1993b, Análisis geoquímico-isotópico de las especies carbónicas del fluido geotérmico de Los Humeros, Puebla, México: Geofísica Internacional, 32(2), 299–309. http://dx.doi.org/10.1515/9781501509650-004

González-Partida, E., Barragán-Reyes, R.M, Vázquez-Escobedo, R., 1992a, Distribución y condiciones de formación de los minerales de arcilla en un campo geotérmico – El caso de Los Humeros, Puebla: Boletín del Instituto de Geología, Universidad Nacional Autónoma de México, 10(1), 47–53.

González-Partida, E., Nieva, G.D., Barragán, R.M., Quijano, J.L., López-Mendiola, J., Gutiérrez, H., 1992b, Comportamiento de las especies sulfurosas en cuatro pozos del Campo Geotérmico de Los Humeros, Puebla, México: Geotermia. Revista Mexicana de Geoenergía, 8, 67–80.

Guiza, J., 1977, Problemas en la Operación en los Pozos Geotérmicos: Boletín Energético, 1, 13–20.

Gutiérrez, L.C., Viggiano, J.C., 1990, Corrosion and Scaling in Well H-16 of the Los Humeros Geothermal Field: Geothermal Resources Council Transactions, 14, 1591–1598.

Gutiérrez-Negrín, C.A., 2007, 1997-2006: A decade of geothermal power generation in Mexico: Geothermal Resources Council Transactions, 31, 167-171.

International Association for the Properties of Water and Steam (IAPWS), 2007, Revised Release on the IAPWS Industrial Formulation 1997 for the Thermodynamic Properties of Water and Steam (The revision only relates to the extension of region 5 to 50 MPa): Lucerne, Switzerland, International Association for the Properties of Water and Steam, Technical Document.

Izquierdo-Montalvo, G., Arellano, V.M., Portugal, E., Aragón, A., Martínez, I., 2000, Acidez de los fluidos del yacimiento geotérmico de Los Humeros, Puebla, México: evaluación mineralógica: Geotermia. Revista Mexicana de Geoenergía, 16 (1-3), 35–44.

Izquierdo-Montalvo, G., Aragón-Aguilar, A., Gómez-Mendoza, F.R., López-Blanco, S., 2014, Evidencia mineralógica del efecto de fluidos ácidos sobre las rocas del yacimiento geotérmico de Los Humeros, Puebla: Geotermia. Revista Mexicana de Geoenergía, 27(1), 3-11.

Lasaga, A., 1995, Fundamental approaches in describing mineral dissolution and precipitation rates, in White A. and Brantley S. (eds.), Chemical Weathering Rates of silicate Minerals, Washington, DC, 23–86. http://dx.doi.org/10.1515/9781501509650-004

Lasaga, A., 1998, Kinetic Theory in the Earth Sciences. Princeton, Princeton, New Jersey. http://dx.doi.org/10.1515/9781400864874

Lichti, K., White, S., McGavin, P., 2005, Software for Geothermal Corrosion and Risk Based Assessment, in Proceedings World Geothermal Congress 2005, Antalya, Turkey, 1–10.

López-Hernández, A., 1995, Estudio regional volcánico y estructural del Campo Geotérmico de Los Humeros, Puebla, México: Geotermia. Revista Mexicana de Geoenergía, 11(1), 17–36.

Martínez-Serrano, R.G., Aliberti, C., 1994, Características geoquímicas de las rocas volcánicas del sistema geotérmico Los Humeros,

http://dx.doi.org/10.18268/BSGM2024v76n1a020124

Puebla y su relación con la mineralogía de alteración: Geofísica Internacional, 33(4), 585–605.

Martínez-Serrano, R.G., 2005, Chemical variations in hydrothermal minerals of the Los Humeros geothermal system, Mexico: Geothermics, 31(5), 579–612. http://dx.doi.org/10.1515/9781400864874

Mena, M., González-Morán, T., 1978, Regional gravity of Los Humeros volcanic area: Geofísica Internacional, 17(4), 429–443. https://doi.org/10.22201/igeof.00167169p.1978.17.4.962

Mercado, S., Bermejo, F., Hurtado, R., Terrazas, B., Bolívar, L., 1989, Scale incidence on production pipes of Cerro Prieto Geothermal Wells: Geothermics, 18(1-2), 225–232. https://doi.org/10.1016/0375-6505(89)90031-X

Miranda-Herrera, C.A., 2012, Silica Scaling Mechanism at Cerro Prieto: GRC Transactions, 36, 1151–1153.

Ocampo-Díaz, J.D., Quintero-Nuñez, M., Moya-Acosta, S.L., 2005, Silica scaling as a predominant factor of the production in Cerro Prieto geothermal wells, Mexico, in Proceedings World Geothermal Congress 2005, Antalya, Turkey, 1–5.

Palacios, H.L., García, H., 1981, Informe geofísico del proyecto geotérmico Los Humeros-Las Derrumbadas: Estados de Puebla y Veracruz, Comisión Federal de Electricidad, informe interno, 96.

Palandri, J.L., Kharaka, Y.K., 2004, A compilation of rate parameters of water-mineral interaction kinetics for application to geochemical modeling: U.S. Geological Survey. Open File Report (of 2004-1068). Prepared in cooperation with the National Energy Technology Laboratory – United States Department of energy.

Pandarinath, K., Rivas-Hernández, J.L., Arriaga-Fuentes, J.A., Yañez-Dávila, D., González-Partida, E., Santoyo, E., 2023, Hydrothermal alteration of surficial rocks at Los Humeros geothermal field, Mexico: A magnetic susceptibility approach: Arabian Journal of Geosciences, 16, 259. https://doi.org/10.1007/s12517-023-11306-3

Pérez, J., 1978, Geología y petrografía de los Humeros: Geomimet, 91, 97–106.

Pérez, R.J., Heidemann, R.A., Pérez, E.C., 2012, A new approach to multiphase geochemical speciation modelling: Applied Geochemistry, 27(9), 1724–1737. https://doi.org/10.1016/j.apgeochem.2012.02.008

Pérez, R., Gimón, R., Cermeño, W., Mosqueda, J., 2017, Simulador de Flujo Bifásico y Flujo de Calor ascendente en tuberías de Producción: Geothermal-pipe Flow: Juriquilla, Querétaro, México, Centro de Geociencias, Universidad Nacional Autónoma de México, Informe de avance de proyecto CONACYT.

Prol-Ledesma, R.M., 1998, Pre- and post-exploitation variations in hydrothermal activity in Los Humeros geothermal field, Mexico: Journal of Volcanology and Geothermal Research 83(3-4), 313–333. https://doi.org/10.1016/S0377-0273(98)00024-9

Prol-Ledesma, R.M., Browne, P.R.L., 1989a, Hydrothermal alteration and fluid inclusion geothermometry on Los Humeros geothermal field, Mexico: Geothermics 18(5-6), 667–690. https://doi.org/10.1016/0375-6505(89)90100-4

Prol-Ledesma, R.M., Browne, P.R.L., 1989b, Fluid inclusions in core samples from the Los Humeros geothermal field, Mexico: Geothermal Resources Council Transactions, 12, 197–202.

Quijano, J.L., Torres, M., 1995, The Los Humeros geothermal reservoir, a case of very high temperature system, in Proceeding of the World Geothermal Congress 1995, Florence, Italy 1596–1573.

Tello, H., Verma, M., Tovar, A., 2000, Origin of acidity in the Los Humeros, México, geothermal reservoir, in Proceedings World Geothermal Congress 2000: Kyushu-Tohoku, Japan, 2959–2967.

Tello, H.E., 1992, Características geoquímicas e isotópicas de los fluidos producidos por los pozos de Los Humeros, Puebla: Geotermia. Revista Mexicana Geoenergía 8, 3–48.

Torres, M., 1995, Characterization of the Reservoir of the Los Humeros, Mexico, Geothermal Field, in Proceeding of the World Geothermal Congress 1995: Florence, Italy, 1561–1567.

Truesdell, A.H., 1991, Origins of acid fluids in geothermal reservoirs: Gordon Research Conference Transactions, 15, 289–296.

Valdez, B., Schorr, M., Quintero, M., Carrillo, M., Zlatev, R., Stoycheva, M., Ocampo, J., 2009, Corrosion and scaling at Cerro Prieto geothermal field: Anti-Corrosion Methods and Materials, 56(1), 28–34. https://doi.org/10.1108/00035590910923437

Van den Heuvel, D.B., Gunnlaugsson, E., Gunnarsson, I., Stawski, T.M., Peacock, C.L., Benning, L.G., 2018, Understanding amorphous silica scaling under well-constrained conditions inside geothermal pipelines: Geothermics, 76, 231–241. https://doi.org/10.1016/j.geothermics.2018.07.006

Viggiano-Guerra, J.C., 1988, Control Petrológico en el Pozo H-26: sus posibilidades de producción: Geotermia. Revista Mexicana de Geoenergía, 4, 123–138.

Viggiano-Guerra, J.C., Flores-Armenta, M.C., Rocha-López, V.S., Sandoval-Medina, F., 2013, Estudio petrográfico del pozo H-43, Los Humeros, Puebla: Interpretación e indicadores mineralógicos de acidez: Geotermia. Revista Mexicana de Geoenergía, 26, 52–61.

Viggiano-Guerra, J.C., Robles-Camacho, J., 1988a, Mineralogía hidrotermal en el campo geotérmico de Los Humeros, Pue. I: Sus usos como indicadora de temperatura y del régimen hidrológico: Geotermia. Revista Mexicana de Geoenergía, 4(1), 15–28.

Viggiano-Guerra, J.C., Robles-Camacho, J., 1988b, Mineralogía hidrotermal en el campo geotérmico de Los Humeros, Pue. II: Geometría del yacimiento: Geotermia. Revista Mexicana de Geoenergía 4(1), 29–40.

White, S., Lichti, K., Bacon, L., 2000, Application of chemical and wellbore modelling to the corrosion and scaling properties of deep wells, in Proceedings World Geothermal Congress 2000: Kyushu-Tohoku, Japan, 3963–3968.

Yáñez-Dávila, D., 2018, Procesos de interacción agua-roca en el reservorio geotérmico de alta entalpía Los Humeros, Puebla, México: Ciudad de México, México, Universidad Nacional Autónoma de México, Tesis de Maestría, p. 94.

Yáñez-García, C., García-Duran, S., 1980, Exploración de la región geotérmica Los Humeros-Las Derrumbadas estados de Puebla y Veracruz: Ciudad de México, México, Comisión Federal de Electricidad, 9.

Yañez, C., García, S., Cacique, J., 1979, Geothermic exploration in the Humeros-Derrumbadas area: Geothermal Resources Council Transactions, 3, 801–803.